Research Paper

PAIN 166 (2025) 773–792

OPEN

$Na_V1.8/Na_V1.9$ double deletion mildly affects acute pain responses in mice

Marta Alves-Simões[a], Laura Teege[b], Cecilia Tomni[c], Martha Lürkens[d], Annika Schmidt[d], Federico Iseppon[a], Queensta Millet[a], Samuel Kühs[b], Istvan Katona[e], Joachim Weis[e], Stefan H. Heinemann[f], Christian A. Hübner[c], John Wood[a], Enrico Leipold[b], Ingo Kurth[d], Natja Haag[d,*]

Abstract

The 2 tetrodotoxin-resistant (TTXr) voltage-gated sodium channel subtypes $Na_V1.8$ and $Na_V1.9$ are important for peripheral pain signaling. As determinants of sensory neuron excitability, they are essential for the initial transduction of sensory stimuli, the electrogenesis of the action potential, and the release of neurotransmitters from sensory neuron terminals. $Na_V1.8$ and $Na_V1.9$, which are encoded by *SCN10A* and *SCN11A*, respectively, are predominantly expressed in pain-sensitive (nociceptive) neurons localized in the dorsal root ganglia (DRG) along the spinal cord and in the trigeminal ganglia. Mutations in these genes cause various pain disorders in humans. *Gain-of-function* missense variants in *SCN10A* result in small fiber neuropathy, while distinct *SCN11A* mutations cause, i. a., congenital insensitivity to pain, episodic pain, painful neuropathy, and cold-induced pain. To determine the impact of *loss-of-function* of both channels, we generated $Na_V1.8/Na_V1.9$ double knockout (DKO) mice using clustered regularly interspaced short palindromic repeats/Cas-mediated gene editing to achieve simultaneous gene disruption. Successful knockout of both channels was verified by whole-cell recordings demonstrating the absence of $Na_V1.8$- and $Na_V1.9$-mediated Na^+ currents in $Na_V1.8/Na_V1.9$ DKO DRG neurons. Global RNA sequencing identified significant deregulation of C-LTMR marker genes as well as of pain-modulating neuropeptides in $Na_V1.8/Na_V1.9$ DKO DRG neurons, which fits to the overall only moderately impaired acute pain behavior observed in DKO mice. Besides addressing the function of both sodium channels in pain perception, we further demonstrate that the null-background is a very valuable tool for investigations on the functional properties of individual human disease-causing variants in $Na_V1.8$ or $Na_V1.9$ in their native physiological environment.

Keywords: $Na_V1.8$, $Na_V1.9$, Acute pain, CRISPR, Knockout, Voltage-gated sodium channel

1. Introduction

Voltage-gated sodium (Na_V) channels play a crucial role in pain transmission. $Na_V1.7$, $Na_V1.8$, and $Na_V1.9$ are the most abundant Na_V subtypes in nociceptive neurons of enteric, trigeminal, and dorsal root ganglia (DRG) with $Na_V1.8$ and $Na_V1.9$ being the main tetrodotoxin-resistant (TTXr) isoforms.[8,28] The essential role of these channels in pain perception is emphasized by various mutations in the *SCN9A*, *SCN10A*, and *SCN11A* genes (encoding $Na_V1.7$, $Na_V1.8$, and $Na_V1.9$, respectively) that underlie a whole spectrum of human disorders ranging from congenital pain insensitivity to painful neuropathic conditions,[8,21] making these channels attractive targets for analgesic research.

Although the structure of Na_V channels is highly conserved, they exhibit distinct functional properties such as different voltage dependencies and gating kinetics, and are thus differentially involved in action potential electrogenesis.[54,57] $Na_V1.7$ is characterized by a relatively hyperpolarized voltage dependence of activation, steady-state inactivation, and fast inactivation kinetics.[17,30] By contrast, $Na_V1.8$ and $Na_V1.9$ exhibit markedly different gating properties.[16] Compared to $Na_V1.7$, $Na_V1.8$ channels activate and inactivate at more depolarized membrane potentials and inactivate more slowly,[3,20] whereas $Na_V1.9$ channels are characterized by a hyperpolarized voltage dependence of activation, steady-state inactivation, and ultraslow inactivation kinetics.[16] Because of these properties, $Na_V1.7$ and $Na_V1.9$ are predominantly active in the initial phase of the action potential and amplify subthreshold stimuli, while $Na_V1.8$ mediates most of the Na^+ current underlying the rapid upstroke of action potentials and supports high-frequency firing in DRG neurons.[11,14,54] In addition to distinct functional properties, $Na_V1.7$, $Na_V1.8$, and $Na_V1.9$

Sponsorships or competing interests that may be relevant to content are disclosed at the end of this article.

M. Alves-Simões, L. Teege, and C. Tomni shared first-authorship.

[a] Molecular Nociception Group, Wolfson Institute for Biomedical Research, University College London, Gower Street, London, United Kingdom, [b] Center of Brain, Behavior and Metabolism & Clinic for Anesthesiology and Intensive Care, University of Lübeck, Lübeck, Germany, [c] Institute of Human Genetics, Jena University Hospital, Friedrich Schiller University, Jena, Germany, [d] Institute for Human Genetics and Genomic Medicine, Medical Faculty, RWTH Aachen University, Aachen, Germany, [e] Institute of Neuropathology, Medical Faculty, RWTH Aachen University, Aachen, Germany, [f] Department of Biophysics, Center for Molecular Biomedicine, Friedrich Schiller University Jena and Jena University Hospital, Jena, Germany

**Corresponding author. Address: Institute for Human Genetics and Genomic Medicine, Medical Faculty, RWTH Aachen University, Aachen, Germany. Tel.: +49 (0)241 80 89913; fax: +49 (0)241 80 82580. E-mail address: nhaag@ukaachen.de (N. Haag).*

Supplemental digital content is available for this article. Direct URL citations appear in the printed text and are provided in the HTML and PDF versions of this article on the journal's Web site (www.painjournalonline.com).

http://dx.doi.org/10.1097/j.pain.0000000000003411

distribution and expression levels also vary among DRG neuron subtypes and between species,[28] further increasing complexity. Several studies have characterized the expression profile of Na_V channels, consistently showing ubiquitous and robust $Na_V1.7$ expression across all DRG neuron subtypes in rodents (mouse, rat, guinea pig), primates, and humans.[10,28,31,51] In contrast, the expression of $Na_V1.8$ and $Na_V1.9$ is more restricted to unmyelinated small-diameter C-fiber neurons across species.[5,28] The individual knockout (KO) of $Na_V1.8$ and $Na_V1.9$ in mice revealed a role of these channels in inflammatory pain, noxious mechanical sensitivity, and cold sensitivity, which is consistent with their overlapping expression in C-fiber DRG neurons.

Although the impact of the simultaneous deletion of $Na_V1.7$ and $Na_V1.8$ for the development of neuropathic pain has been described,[51] the effects of the concomitant deletion of both $Na_V1.8$ and $Na_V1.9$ channels on pain transmission have not yet been explored. This is primarily because of the genomic proximity of the corresponding genes *Scn10a* and *Scn11a*, which are genetically linked because they are located nearby on chromosome 9 in mice (chromosome 3 in humans). To further investigate the roles of $Na_V1.8$ and $Na_V1.9$ in pain transmission, we generated $Na_V1.8$/$Na_V1.9$ double knockout (DKO) mice using a clustered regularly interspaced short palindromic repeats (CRISPR)/Cas9 strategy, characterized their pain phenotype, and demonstrate that $Na_V1.8$/$Na_V1.9$ DKO neurons have advantages to study human wild-type (WT) and mutant $Na_V1.8$ and $Na_V1.9$ channels in DRGs.

2. Material and methods

2.1. Animal ethics statement

All animal procedures were approved by the local government (approval no. 02-028/14; *Thüringer Landesamt*, Bad Langensalza, Germany; approval no. 81-02.04.2019.A358; *Landesamt für Natur, Umwelt und Verbraucherschutz*, North Rhine-Westphalia, Recklinghausen, Germany; and in accordance to the UK Animals (Scientific Procedures) Act 1986 under a Home Office project license no. P413329A2). For data evaluation of acute pain behavior tests, we adhered to the ARRIVE guidelines (https://arriveguidelines.org/).

2.2. Generation of $Na_V1.8$/$Na_V1.9$ double knockout mice

2.2.1. Cloning

The bicistronic expression vector pX330-U6-chimeric_BB-CBh-hSpCas9 (Addgene #42230, Watertown, MA) expressing human codon–optimized Cas9 (hSpCas9) and a single guide RNA (sgRNA) cloning site[15] was digested with BbsI, and the linearized vector was gel-purified. A pair of partially complementary DNA oligos, containing the 20-nt-sgRNA sequence and 4-nt-overhangs compatible for cloning into the vector, was designed for each targeting site using Benchling (www.benchling.com) (see Supplementary Table 1, http://links.lww.com/PAIN/C139). Oligo annealing was performed by mixing 30 μL each of the respective forward/reverse primer stock solutions (100 pmol/μL), overlayed with paraffin oil, placed in boiling water, and cooled down for at least 3 hours. Annealed oligos were ligated into the pX330 vector, and final constructs were checked for correct insertion by sequencing.

2.2.2. sgRNA in vitro transcription

For injection into zygotes, sgRNAs were synthesized by in vitro transcription (IVT) using the MEGAshortscript T7 Transcription Kit (Thermo Fisher Scientific, Waltham, MA) following the manufacturers' instructions. Because pX330 plasmids lack a classical RNA Polymerase III promoter, 120-bp polymerase chain reaction (PCR) products containing T7 promoter, target, and scaffold sequence were generated using T7-sgRNA forward (fwd; F) and reverse (rev; R) primers (see Suppl. Table 1, http://links.lww.com/PAIN/C139) together with 15 ng of pX330 plasmid and amplified with Herculase II Fusion DNA Polymerase (Agilent, Santa Clara, CA). PCR products were gel-purified, concentrated (DNA Clean & Concentrator Kit, Zymo Research Europe, Freiburg, Germany), and eluted into nuclease-free distilled water. The sgRNAs were purified using the MEGAclear Transcription Clean-Up Kit (Thermo Fisher Scientific). Before injection into zygotes, sgRNA integrity was checked by RNA gel electrophoresis.

2.3. One-cell embryo injection

Microinjection of CRISPR constructs into zygotes was performed following standard procedures.[50] Zygotes were obtained from superovulated female C57BL6/J mice. Immediately after receiving one human chorionic gonadotropin (hCG) injection, superovulated females were mated to C57BL/6 males. Fertilized eggs were collected the next day from oviducts and kept in Krebs-Ringer Bicarbonate Buffer at 37°C until the appearance of both female and male pronuclei. Then, zygotes were transferred to Krebs-Ringer Bicarbonate Buffer/20 mM HEPES, and PrecisionX Cas9 SmartNuclease mRNA (eukaryotic version, System Biosciences, Palo Alto, CA) plus a mixture of the 4 transcribed sgRNAs was injected into the pronucleus or cytoplasm. Injected zygotes were cultured further, and only two-cell-stage embryos were transferred into the oviduct of pseudo-pregnant foster mothers (0.5 days postcoitus).

2.4. Off-target analysis

Off-target (OT) sequences were computationally identified and ranked using Benchling (www.benchling.com), allowing for up to 4 mismatches in the target gRNA sequence. For each sgRNA, primers for the top 5 OT sequences and OT coding regions, if detected, were designed (see Supplementary Table 2, http://links.lww.com/PAIN/C139). PCR amplification was performed from DNA of the founder chimaera and the 2 F1 founder animals to determine if any mutations or changes occurred in OT sites using HotStarTaq Plus DNA Polymerase (Qiagen, Hilden, Germany).

2.5. Mouse genotyping

Genotyping of $Na_V1.8$/$Na_V1.9$ DKO mice was performed with exon-specific primers (see Supplementary Table 3, http://links.lww.com/PAIN/C139) and HotStarTaq Plus DNA Polymerase (Qiagen). DNA was extracted from tail biopsies using the HotSHOT method.[73] PCR products were analyzed by agarose gel electrophoresis and nondenaturing polyacrylamide gel electrophoresis (PAGE) and sequenced.

2.6. Quantitative real-time PCR

Immediately upon isolation, DRGs were frozen in liquid nitrogen and ground with a mortar and pestle into powder using liquid nitrogen. Using TRIzol reagent (Thermo Fisher Scientific), RNA was isolated according to manufacturer's protocol. RNA quality was assessed using a Nanodrop 2000 Spectrophotometer (Thermo Fisher Scientific). cDNA was synthesized from 1 μg

RNA using the Maxima First Strand cDNA Synthesis Kit for real-time-quantitative polymerase chain reaction (RT-qPCR) (Thermo Fisher Scientific), of which 25 ng of cDNA was used per qPCR reaction. qPCR was performed for 40 cycles at an annealing temperature of 60°C using the PowerUp SYBR Green Kit on a StepOnePLus Real-Time PCR System (Applied Biosystems, Thermo Fischer Scientific). All samples were run in duplicate. Primer sequences are listed in Supplementary table 4, http://links.lww.com/PAIN/C139. The detected cycle-threshold values (Ct) were normalized to Ct values of the housekeeping genes *B2m* and *β-actin*. Data were calculated using the ΔΔCt method. Gene expression changes are specified as fold changes in comparison to the average WT gene expression, normalized to *B2m*- and *β-actin*-expression.

2.7. RNA sequencing

2.7.1. Tissue preparation

Dorsal root ganglia were taken from 6 male and 6 female mice (3 WT, 3 DKO animals each, 22-35 week old), snap-frozen on dry ice, and stored at −80°C. The DRG dissection procedure was performed as described.[24]

2.7.2. RNA extraction

RNA from snap-frozen DRGs was extracted using NucleoZOL (Macherey-Nagel, Germany) according to manufacturer's instructions. Concentration and purity were determined by spectrophotometry (NanoDrop 2000), and RNA integrity was measured by capillary gel electrophoresis (RNA ScreenTape, Agilent Technologies) according to manufacturer's protocol. Samples with RNA Integrity Numbers (RIN) values above 8.0 were used for RNA sequencing.

2.7.3. Next-generation RNA sequencing

For generating complementary DNA (cDNA) libraries for RNA-sequencing, NEBNext rRNA Depletion Kit (Human/Mouse/Rat), NEBNext Ultra II Directional RNA Library Prep Kit, NEBNext rRNA Depletion Kit v2 (Human/Mouse/Rat), and NucleoMag NGS Clean-Up Beads (Macherey-Nagel, 744970.50) were used. Library quality assessment was performed with capillary gel electrophoresis (TapeStation, Agilent). Based on the results, samples were diluted to 1 nM with 10 mM of Tris-HCl (pH 8.5) supplemented with 0.1% Tween and then pooled by mixing 10 μL of each sample. Pooled libraries were stored at −20°C. Sequencing was performed on a High Output 1 × 75 Flowcell on a NextSeq 500 sequencer (Illumina, San Diego, CA). Sequencing results were aligned to the *Mus musculus* reference genome (GRCm39/mm39) with an in-house customized pipeline using STAR aligner.

Computational analysis was performed with R in RStudio (4.2.3). Overall data quality was assessed using a principal component analysis. Differential gene expression analysis was performed with a standard DESeq2 pipeline and further investigated by performing a gene ontology-analysis using gprofiler2.

2.8. Isolation and transfection of mouse dorsal root ganglia neurons

Dorsal root ganglia from all levels of the spinal cord of 8 to 12-week-old wild-type and $Na_V1.8$/$Na_V1.9$ DKO mice were isolated using standard procedures[24] and processed as described previously[36] with minor modifications. Briefly, approximately 30 DRGs per animal were isolated, freed from all distal and central processes, and collected in a 1.5-mL microcentrifuge tube filled with 1.4-mL ice-cold complete saline solution (CSS) containing 137 mM of NaCl, 5.3 mM of KCl, 1 mM of $MgCl_2$, 25 mM of sorbitol, 10 mM of HEPES, and 3 mM of $CaCl_2$ (pH 7.2 with NaOH). Isolated ganglia were washed once with CSS followed by digestion in 1.4 mL of CSS buffer supplemented with 0.5 U Liberase Blendzyme TH (F. Hoffmann-La Roche, Basel, Switzerland), 30 U papain (Sigma-Aldrich, St. Louis, MO), and 0.5 mM EGTA for 25 to 30 minutes at 37°C. Subsequently, ganglia were pelleted in a centrifuge at 250*g* for 2 minutes. After removing the supernatant, DRGs were resuspended in 980 μL of Accutase (Sigma-Aldrich) and 420 μL of CSS, supplemented with 0.5 U Liberase Blendzyme TM (F. Hoffmann-La Roche, Basel, Switzerland) and 0.5 mM of EDTA, and digested at 37°C for an additional 15 to 20 minutes. Digested ganglia were centrifuged again at 250*g* for 2 minutes, and the supernatant was removed. To stop the digestion process and to obtain a single-cell suspension, the pellet was resuspended in 0.5 mL of DMEM/F12 culture medium (Pan-Biotech GmbH, Aidenbach, Deutschland) containing 1.5 mg/mL of BSA (Sigma-Aldrich) and 1.5 mg/mL of trypsin inhibitor (F. Hoffmann-La Roche, Basel, Switzerland) followed by trituration using a 1-mL Pipetman and 10 to 15 strokes. The resulting single-cell suspension was then centrifuged at 250*g* for 3 minutes, and the supernatant was discarded.

For experiments with nontransfected neurons, isolated cells were resuspended in 500 μL of DRG medium composed of 89.5% DMEM/F12, 9.5% fetal bovine serum (Biochrom GmbH, Berlin, Deutschland), and 1% penicillin/streptomycin (Biochrom GmbH) and immediately seeded on poly-L-lysin–coated glass coverslips, which were placed in the slots of a 24-well plate containing 1 mL of DRG medium per well. Cells were incubated for 24 to 48 hours at 37°C in a 5% CO_2 incubator before being used for electrophysiological experiments.

To overexpress human Na_V channels, isolated DRG neurons were transfected by electroporation using a 4D-Nucleofector (Lonza, Basel, Switzerland) with the P3 Primary Cell 4D-Nucleofector Kit (V4XP-3032) according to the manufacturer's recommendations. Briefly, dissociated DRG neurons obtained from one animal were washed once with 0.5 mL of Ca^{2+}- and Mg^{2+}-free PBS and then resuspended in 20 μL of P3 primary cell solution containing supplement 1 (both Lonza) and 1.5 to 2.5 μg of a plasmid encoding either $hNa_V1.8$, $hNa_V1.9$, or $hNa_V1.9$-L811P. The 3 plasmids had a two-promoter architecture enabling the simultaneous expression of either $hNa_V1.8$, $hNa_V1.9$, or $hNa_V1.9$-L811P under the control of the CMV promoter and enhanced green fluorescent protein (eGFP) under the control of the SV40 promoter. Transfection was performed using the electroporation protocol CA137 of the 4D-Nucleofector device. Immediately after electroporation, 150 μL of low calcium RPMI 1640 medium (Gibco by Thermo Fisher Scientific) was added to the suspension, and cells were allowed to recover for 10 minutes at 37°C in a 5% CO_2 incubator before they were seeded on glass coverslips as mentioned above. Electrophysiological recordings were performed 24 to 48 hours post transfection. Recordings were restricted to successfully transfected small-diameter (<30 μm) neurons, which were identified by their bright green fluorescence using a pE-300 LED light source (CoolLED Ltd., Andover, United Kingdom) and a green fluorescent protein filter set (AHF Analysentechnik AG, Tübingen, Germany).

2.9. Electrophysiology

Voltage- and current-clamp recordings were obtained in the whole-cell configuration of the patch-clamp method using an

EPC10 patch-clamp amplifier operated by PatchMaster software (HEKA Elektronik, Lambrecht, Germany). All recordings were performed at a constant temperature of 20 ± 0.5°C using a microincubation stage (ALA Scientific Instruments, Farmingdale, NY) feedback-controlled by a PTC-10 temperature controller (NPI Electronic GmbH, Tamm, Germany). Patch pipettes were fabricated from borosilicate glass capillaries and coated with silicone elastomer (RTV 615, Momentive Performance Materials, Waterford, NY) to reduce tip capacitance. Series resistance was corrected electronically up to 90%. Bath solution for voltage-clamp recordings in nontransfected DRG neurons contained (in mM) 35 NaCl, 95 cholin-Cl, 2 KCl, 2.5 $CaCl_2$, 1 $MgCl_2$, 10 HEPES, 20 TEA-Cl, and 1 4-Aminopyridine P, 0.1 $CdCl_2$ (pH 7.4. with NaOH). Tetrodotoxin (Alomone Labs, Jerusalem, Israel) was dissolved in bath solution to a final concentration of 1 μM and applied locally to cells with a glass pipette as described earlier.[35] The corresponding pipette solution contained (in mM) 10 NaCl, 130 CsF, 10 EGTA, and 10 HEPES (pH 7.4 with CsOH). For voltage-clamp recordings of $hNa_V1.8$, $hNa_V1.9$, and $hNa_V1.9$-L811P channels heterologously expressed in $Na_V1.8/Na_V1.9$ DKO DRG neurons, the bath contained (in mM) 130 NaCl, 2 KCl, 2.5 $CaCl_2$, 1 $MgCl_2$, 10 HEPES, 20 TEA-Cl, 1 4-Aminopyridine, and 0.1 $CdCl_2$ (pH 7.4. with NaOH) and was supplemented with 0.001 TTX to completely block tetrodotoxin-sensitive (TTXs) Na_V channels endogenous to $Na_V1.8/Na_V1.9$ DKO DRG neurons; the corresponding pipette solution contained (in mM) 10 NaCl, 130 CsF, 10 EGTA, and 10 HEPES (pH 7.4 with CsOH). Bath solution for current-clamp recordings contained (in mM) 120 NaCl, 3 KCl, 2.5 $CaCl_2$, 1 $MgCl_2$, 30 HEPES, 15 glucose (pH 7.4 with NaOH), and the pipette 125 KCl, 8 NaCl, 1 $CaCl_2$, 1 $MgCl_2$, 0.4 Na_2-GTP, 4 Mg-ATP, 10 EGTA, 10 HEPES (pH 7.3 with KOH). All electrophysiological recordings were analyzed with FitMaster (HEKA Elektronik) and IgorPro (WaveMetrics, Lake Oswego, OR) software.

2.9.1. Voltage-clamp recordings

For voltage-clamp recordings, the holding potential was set to −130 mV. Data were low-pass filtered at 3 kHz and sampled at an interval of 40 μs. Leak and capacitive currents were recorded using a P/6 protocol with 6 leak pulses, each with 0.15 time the amplitude of the test pulse P. Summed and scaled leak traces were subtracted online using the leak pulse feature available in PatchMaster software. The liquid junction potential was not corrected.

2.9.2. Na_V channel activation

Activation of Na_V channels was measured with test depolarizations ranging from −120 to 40 mV applied in steps of 10 mV. The voltage dependence of channel activation was estimated from peak current densities using the following formalism:

$$\frac{I(V)}{C_m} = \Gamma \cdot (V - E_{rev}) \cdot \frac{1}{1 + e^{-(V - V_m)/k_m}} \quad (1)$$

with the cell membrane capacitance C_m, conductance density Γ, and the reversal potential (E_{rev}). V_m is the half-maximal activation voltage and k_m the corresponding slope factor.

2.9.3. Na_V channel steady-state inactivation

Na_V channels in nontransfected wild-type and $Na_V1.8/Na_V1.9$ DKO DRG neurons were activated with a first 50-ms test pulse to −20 mV followed by a conditioning interval of 500 ms at voltages ranging from −140 to 0 mV in steps of 10 mV. Peak currents of not inactivated channels were measured in a subsequent 50-millisecond test pulse to −20 mV. The repetition interval was 10 seconds. For $hNa_V1.8$, $hNa_V1.9$, and $hNa_V1.9$-L811P channels overexpressed in $Na_V1.8/Na_V1.9$ DKO DRG neurons, test pulse voltages were −10 mV, −40 mV, and −60 mV, respectively, accounting for the different voltage-dependent activation properties of these channels. For all experimental conditions, the current amplitude after conditioning (I_{500}) normalized to the control current amplitude before conditioning (I_0) was described with the following Boltzmann formalism:

$$\frac{I_{500}}{I_0} = h_{max} - (h_{max} - h_{min}) \cdot \left(\frac{1 - P}{1 + e^{-(V - V_h)/k_h}} + \frac{P}{1 + e^{-(V - V_{hp})/k_{hp}}} \right)$$

with h_{min} and h_{max} being the minimal and maximal channel availability, respectively, and the half-maximal inactivation voltages V_h and V_{hp} characterizing the inactivation of TTXs and TTXr channels, respectively; k_h and k_{hp} are the corresponding slope factors. For recordings obtained with wild-type DRG neurons in the absence of TTX, P and $1-P$ represent the fractions of TTXr ($Na_V1.8$ and $Na_V1.9$) and TTXs Na_V channels, respectively. To analyze inactivation of Na_V channels in $Na_V1.8/Na_V1.9$ DKO DRG neurons in the absence of TTX, P was set to zero. In all experiments conducted in the presence of TTX, P was set to one.

2.9.4. Inhibition of Na_V channels by tetrodotoxin

Onset of Na_V channel block by 1 μM of TTX and recovery from block were measured with repetitive pulses to 0 mV applied every 1 second. Peak currents, plotted as a function of time, were fitted with a single-exponential function to estimate the time constants characterizing the TTX-mediated current block (τ_{block}), recovery from block ($\tau_{recovery}$), and the steady-state current remaining after TTX equilibration (I_{rem}).

2.9.5. Current-clamp recordings

Current-clamp recordings were obtained from nontransfected wild-type and $Na_V1.8/Na_V1.9$ DKO neurons. The sampling interval was 20 μs. After obtaining the whole-cell configuration in voltage-clamp mode, a brief 50-millisecond test pulse to 0 mV was applied from a holding potential of −60 mV to record total inward and outward currents, which are mostly mediated by the activity of Na_V and voltage-gated potassium channels (K_V channels), respectively.

The impact of the double knockout on functional channel expression was estimated from corresponding peak current densities. Leak and capacitive currents were recorded using a P/n method with 4 hyperpolarizing leak pulses, each with −0.15 times the amplitude of the test pulse P. Summed and scaled leak traces were subtracted using the leak pulse feature available in PatchMaster software. The input resistance of the neurons (R_{in}) was estimated from leak current amplitudes according to Ohm's law. After switching to current-clamp mode, the resting membrane potential (RMP) of cells that did not generate spontaneous action potentials was measured by zero current injection. Subsequently, single action potentials were evoked by injecting a current of 100 to 200 pA for a period of 10 milliseconds, followed by a 400-millisecond period without current injection. Voltage recordings were corrected offline for the liquid junction potential (−7 mV). Parameters characterizing individual action potentials, including action potential peak voltage (V_{max}), maximal after-hyperpolarization (V_{min}), voltage threshold of action potential firing (V_{th}), and action potential width at threshold voltage ($Width_{th}$), were analyzed with Igor Pro software using customized scripts. V_{th} was defined as voltage at which dV/dt reached the level of $0.03 \times (dV/dt_{max} - dV/dt_{min}) + dV/dt_{min}$.[37]

Trains of action potentials were evoked repetitively by 2 seconds current injections, increasing from 0 to 120 pA in steps of 20 pA. Associated firing frequencies were obtained using 0 and −20 mV as action potential detection thresholds.

2.10. Immunohistochemistry and fluorescence microscopy

Cryosections (12 μm) of 4% paraformaldehyde (PFA)-fixed DRG and spinal cord tissue from 2- to 5-month-old mice were stained with antibodies (see Supplementary table 5, http://links.lww.com/PAIN/C139) using standard procedures. Images were acquired with a Zeiss Observer Z.1 microscope equipped with an Apotome2 and HXP 120 lamp (Plan-Apochromat 20x/0.8 objective, ZEN software, version 2.3.69.1000).

2.11. Flow cytometry

Isolated DRGs were enzymatically dissociated by collagenase (0.2% in HBSS, 10 mM HEPES, pH 7.25) treatment for 20 minutes at 37°C followed by another 20 minutes after adding an equal volume of 0.05% Trypsin-EDTA. Dorsal root ganglia were gently triturated in FACS solution (10% Fetal Bovine Serum/FBS in HBSS, 10 mM HEPES, pH 7.25) with fire-polished glass pipettes of decreasing diameter. The resulting single cell suspension was filtered (40 μm cell strainer, BD falcon), washed once in FACS solution, and fixed in 2% PFA in PBS for 10 minutes at room temperature. About 25% (vol/vol) of the single cell suspension was withdrawn and kept on ice (unstained control). The remaining cells were blocked, permeabilized, and stained for 60 minutes at room temperature in block solution (10% FCS, 1% Normal Goat Serum, 0.05% Triton-X100) containing FITC-IB4 (1:100) and mouse anti-CGRP-AlexaFluor647 (1:300) with constant gentle agitation. Measurements were conducted on a FACS Canto II flow cytometer (Becton Dickinson, Heidelberg, Germany).

2.12. Histopathology

Mice (n = 3 per genotype) were sacrificed via CO_2 inhalation and immediately fixed by transcardial perfusion with PBS followed by 3.9% glutaraldehyde/PBS. Tissues (DRGs, spinal cord, sciatic nerve, skin/footpad, muscle (*M. soleus*, *M. gastrocnemius*)) were dissected, embedded in epoxy resin, and further processed for semithin-section light microscopy and ultrathin-section electron microscopy as described previously.[65]

2.13. Behavioral testing

Behavioral measures were acquired as previously described.[44,49] Briefly, mechanical sensitivity was measured using the up-down method with von Frey filaments to the hind paw and increasing mechanical pressure using a modified Randall–Selitto test to the tail with a 500 g cutoff. Thermal thresholds to heat were measured using the Hargreaves test with a heat ramp of 1.5°C/second and by measuring the time to first nociceptive behavior in a 55°C plate test. Cold sensitivity was measured using 3 different tests: cold plate at 5°C for 60 seconds and 10°C for 10 minutes where the time spent lifting or shaking the forepaws was measured; paw-withdrawal latency to the application of dry ice to a glass surface; and behavioral responses during the first minute after the application of a droplet of acetone to the hind paw. In addition, using 2 different adjacent electronic plates set at 3 different temperature combinations (10°C and 0°C, 20°C and 10°C, 30°C and 5°C), the time spent in each plate during a total of 120 seconds was measured to measure thermal place preference. Nocifensive behaviors induced by 5% formalin intraplantar injection were recorded for a period of 60 minutes, and the time spent licking/biting/flinching the injected paw was quantified in 5-minute bins. Each behavior measure was repeated twice by different experimenters blinded to the genotype of the mice. All experiments included males and females aged 8 to 16 weeks. Before pain behavior assessments, mice were examined for motor skills using an accelerating rotarod[18] and open field maze as previously described.[66] The total number of crossings and time spent in the center section of the field were quantified (Supplementary Fig. 9, http://links.lww.com/PAIN/C139).

2.14. Data analysis

Statistical analyses were conducted using GraphPad Prism Version 9.4.1 (GraphPad Software, San Diego, CA) unless otherwise stated. The statistical tests applied are indicated in the legends of the respective figures. Numbers of mice used are also noted in figure legends (typically 2-3 trials per mouse).

3. Results

3.1. CRISPR/Cas-mediated bigenic silencing of the linked Na_V genes Scn10a and Scn11a by cytoplasmic sgRNA/Cas9 mRNA injection

The generation of $Na_V1.8$/$Na_V1.9$ DKO mice by intercrossing $Na_V1.8$ knockout (KO)[3] animals with $Na_V1.9$ KO[6] animals is not feasible because the corresponding genes, *Scn10a* and *Scn11a*, respectively, are both located in close proximity on mouse chromosome 9 with an intergenic distance of only 34.7 kb (UCSC Genome Browser; GRCm39/mm39) and are thus inherited together. Because this also impedes a one-step homologous recombination strategy, CRISPR/Cas9-mediated gene disruption was used for simultaneous gene targeting of *Scn10a* and *Scn11a* in mice. In addition to the classical genomic rearrangements associated with CRSPR/Cas9-activated nonhomologous end-joining (NHEJ) repair, such as deletions and insertions (indels), inversions, duplications, and substitutions near the cleavage site,[15,29] simultaneous targeting of 2 adjacent homologous genes can also cause exon inversions and exon fusions, further increasing the complexity of the editing procedure. Moreover, only editing of alleles on the same chromosome in *cis* are useful to

produce a *Scn10a/Scn11a* double knockout background. Accordingly, the targeting and genotyping strategy had to consider these possible outcomes. Thus, the selected approach involved targeting independent exons in each gene to avoid novel transcripts from gene fusion. Two 20-nt-sgRNAs were designed per gene (see Supplementary table 1, http://links.lww.com/PAIN/C139) targeting exon 6 (Ex6) and exon 11 (Ex11) for *Scn10a*, and exon 9 (Ex9) and exon 10 (Ex10) for *Scn11a* (**Fig. 1A**). The cleavage sites in exons 6 and 11 are separated by 6650 bp, while in exons 9 and 10, they are separated by 1234 bp. A precise deletion of the region between both cuts in each respective gene would lead to a frameshift mutation. Before injection into zygotes, sgRNA efficacy was tested in vitro by performing a plasmid DNA cleavage assay (see Supplementary methods and Supplementary Fig. 1, http://links.lww.com/PAIN/C139).

To verify gene editing specificity, off-target (OT) analysis was performed by PCR of the top 5 OT sequences and OT coding regions for each sgRNA as predicted by Benchling (Supplementary table 2, http://links.lww.com/PAIN/C139). The regions containing the potential OT sites were amplified and further sequenced to determine if any mutations or changes occurred. Only the founder chimera (F_0#11) and 2 F_1 founder animals (F_1#5, F_1#6) were analyzed. A total of 23 OT sites were examined (5 OT sites for *Scn10a*-Ex6, 6 for *Scn10a*-Ex11 and *Scn11a*-Ex9/10 each). Although other potential OT effects cannot be excluded, no *indel* mutation was observed in the analyzed OT regions in any of the mutant mice (Supplementary Fig. 2, http://links.lww.com/PAIN/C139).

3.2. Validation of $Na_V1.8/Na_V1.9$ double knockout

Two F_1 founder animals harboring the allele combination *Scn10a*-Ex11 T > A/Δ 1bp and *Scn11a*-Ex9 Δ 4bp (**Fig. 1B**), supposed to cause premature stops in both genes in *cis*, were further mated to generate the $Na_V1.8/Na_V1.9$ DKO mouse line. Sequencing of F_2 offspring confirmed the correct transmission of the desired alleles, both leading to premature stop codons (**Fig. 1B**). Offspring from heterozygous breeding was born at Mendelian ratio (wild-type, WT: 27.3%, heterozygous, HET: 48.5%, double knockout, DKO: 24.2%; n = 132, P = n.s., χ^2 test) and displayed a normal sex distribution (46.2% females, 53.8% males; P = n.s., binomial test). Body weights of both sexes were unaltered (see Supplementary Fig. 6D, http://links.lww.com/PAIN/C139). Homozygous $Na_V1.8/Na_V1.9$ DKO mice were fertile, displayed normal viability, and did not show apparent abnormalities or deficits during 2 years of monitoring. Thus, lack of both sodium channel α-subunits does not seem to interfere with global embryonic development and life expectancy.

To identify possible compensatory gene regulations in DKO DRG neurons, we performed global RNA sequencing (bulk RNAseq) of whole DRGs obtained from 3 WT and 3 DKO animals (22-35 weeks old). The analysis revealed that *Penk*, *Ano2*, and *Loxhd1* were the only significantly, albeit moderately, upregulated genes in DKO DRGs (**Figs 1C and D**, Supplementary Fig. 3, http://links.lww.com/PAIN/C139). *Penk* encodes the endogenous opioid polypeptide hormone proenkephalin, which is converted to Met- and Leu-enkephalin by proteolytic cleavage. Both neuropeptides are implicated in various physiological functions including the control of pain as they are potent antagonists of the delta-opioid receptor and to a lesser extent also of the mu-opioid receptor.[28,68] *Ano2* (*Tmem16b*) is a member of the anoctamin family of calcium-activated chloride channels (CaCCs) with a reported function in olfactory signal transduction.[69] Consistent with available single-cell transcriptome data showing that *Ano2* mRNA is barely detectable in genetically unmodified DRG neurons,[9,67,74,79] no DRG-specific functions for *Ano2* are known either. On the other hand, *Ano2* was shown to be involved in spike frequency adaptation and regulation of sensory signal transmission in thalamocortical neurons, which relay sensory input, including nociceptive information, from the thalamus to the cortex.[23] However, its close paralog *Ano1* (*Tmem16a*) was shown to be expressed in small nociceptive DRG neurons from rodents[40,77] where it contributes to the neurons' heat sensitivity[13] and to their increased excitability after nerve injury and during inflammatory conditions.[12,34,40] Although *Ano2* mRNA level in DKO-DRG preparations are significantly increased, they are still comparatively low in absolute numbers and, therefore, possibly only of minor physiological significance. Alternatively, *Ano2* upregulation could also be restricted to subpopulations of DRG neurons, associated glial cells, or both, which could be analyzed in the future using single-cell–based sequencing approaches. The *Loxhd1* gene product is predicted to contain 15 PLAT (polycystin-lipoxygenase-α-toxin) domains, which share similarities with Ca^{2+}-binding C2 domains and are thought to be involved in the targeting of proteins to the plasma membrane.[4,7,53] While its function in DRG neurons is unknown, *Loxhd1* is critically involved in mechanotransduction in the auditory system.[72]

By contrast, a total of 47 genes were significantly downregulated. As predicted by gene ontology (GO) enrichment analysis, the downregulated genes are part of gene networks associated with ion transport and cellular excitability (Supplementary Fig. 4, http://links.lww.com/PAIN/C139). As expected, the most affected genes were *Scn10a* and *Scn11a* (**Figs. 1C–E**). The $Na_V1.5$-encoding gene *Scn5a* was also significantly downregulated, albeit to a lesser extent. Similar results were obtained by independent qPCR analysis confirming downregulation of *Scn5a*, *Scn10a*, and *Scn11a* in the neurons (**Fig. 1E**, Supplementary Table 6, http://links.lww.com/PAIN/C139). Among the downregulated genes, there were only 2 others that code for ion channels: *Cacna1i*, encoding the α-subunit of the voltage-gated T-type calcium channel $Ca_V3.3$ (**Figs. 1D and E**), and *Chrna4*, which codes for the α4 subunit of the nicotinic acetylcholine receptor (**Fig. 1D**, Supplementary Fig. 3C, http://links.lww.com/PAIN/C139). However, transcription levels of genes related to TRP channels, GPCRs, or voltage-gated potassium channels were not affected (Supplementary Fig. 3B,D,E, http://links.lww.com/PAIN/C139). In addition, typical marker genes of C-low-threshold mechanoreceptors (C-LMTRs) including *Th*, *Slc17a8*, *Caecam10*, and *Tafa4* were collectively downregulated in DKO DRGs (**Figs. 1C and D**), indicating a loss and/or functional alteration of this sensory neuron subtype in the DKO animals.

In summary, although the $Na_V1.8/Na_V1.9$ double knockout caused deregulation of numerous genes in DRG neurons, it had no obvious effect on the outcome of the animals.

3.3. Dorsal root ganglia neurons of $Na_V1.8/Na_V1.9$ double knockout mice lack functional $Na_V1.8$ and $Na_V1.9$ channels

To verify the successful knockout of $Na_V1.8$ and $Na_V1.9$ at the functional level, whole-cell voltage-clamp recordings were performed in DRG neurons isolated from $Na_V1.8/Na_V1.9$ DKO and WT mice. All recordings were first performed in the absence of TTX to characterize total Na^+ currents containing both TTXs and TTXr components and then repeated after focal application of 1 μM TTX to isolate the TTXr current components mediated by $Na_V1.8$ and $Na_V1.9$.[2,6,63,70]

In wild-type DRG neurons, depolarizing test pulses between −120 mV through 40 mV, incremented in steps of 10 mV, evoked 2 types of Na^+ currents that activated and inactivated with clearly distinguishable kinetics (**Fig. 2A**). While at low voltages mainly slow activating, slow inactivating Na^+ currents

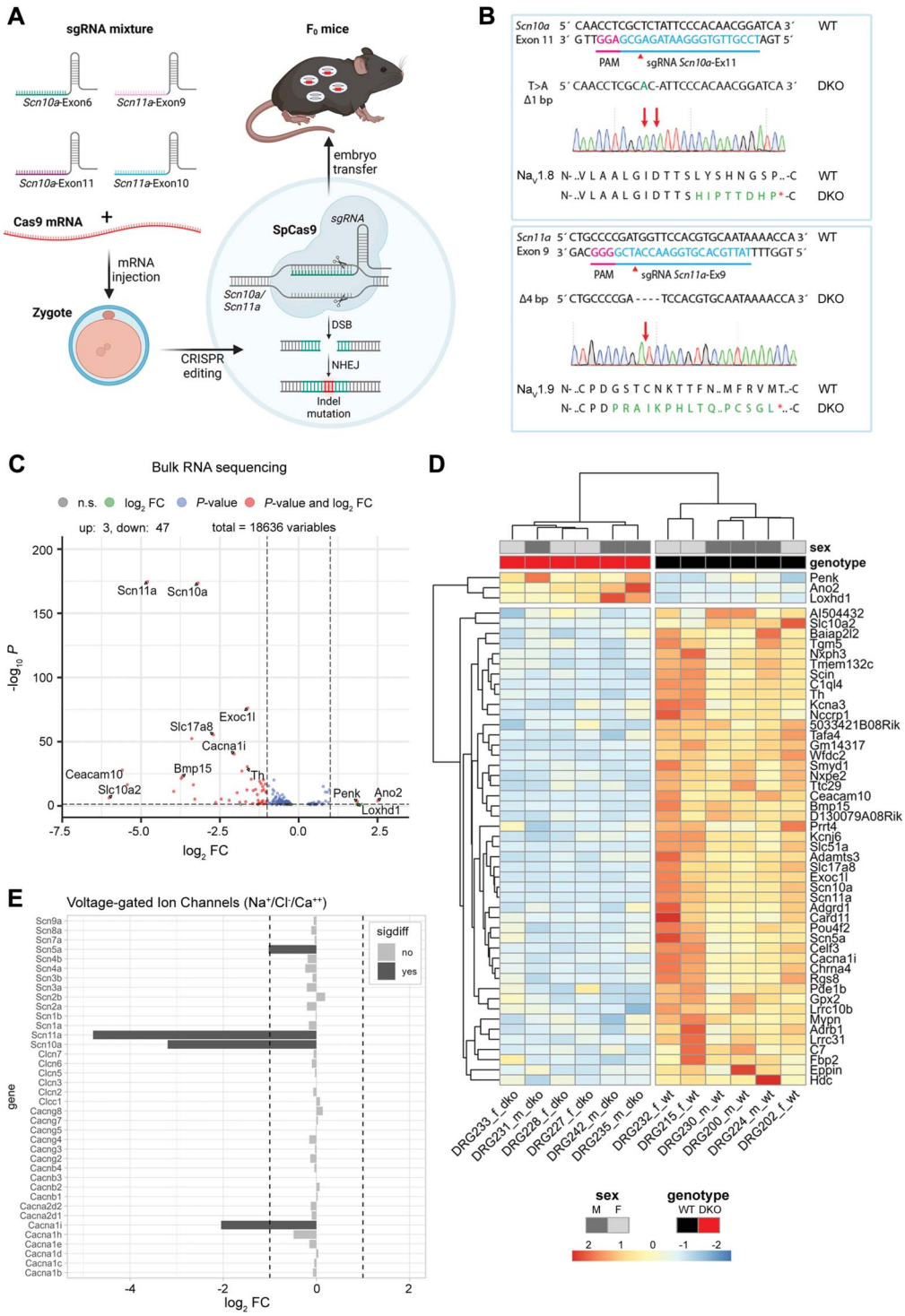

Figure 1. Generation and validation of $Na_V1.8/Na_V1.9$ DKO mice. (A) Schematic representation of the targeting strategy. *Streptococcus pyogenes* Cas9 (SpCas9) mRNA and 4 sgRNAs targeting the respective exons of *Scn10a* and *Scn11a* were microinjected into zygotes aiming for double-strand breaks (DSB) to trigger nonhomologous end joining (NHEJ). (B) Sequencing of DNA obtained from $Na_V1.8/Na_V1.9$ DKO mice confirmed a T > A substitution along with a 1-bp deletion in *Scn10a*-Ex11 plus a 4-bp deletion in *Scn11a*-Ex9. Red arrows indicate the respective mutations in the chromatogram. Both mutations lead to premature stop codons. (C–E) Bulk RNA sequencing from whole DRGs. (C) Volcano plot of differentially expressed genes (DEGs) between $Na_V1.8/Na_V1.9$ DKO and WT mice. The plot shows magnitude of differential expression (x-axis) and significance (y-axis) in logarithmic scales. Dotted lines indicate thresholds of significance (adjusted *P*-value < 0.05) and fold changes (log_2 FC > 1 or log_2 FC < -1). Significantly DEGs are depicted in red, significantly but not differentially expressed genes in blue. Not significantly but differentially expressed genes are depicted in green, or grey, if neither significant nor differentially expressed. (D) Heatmap plot of significantly DEGs between genotypes. Blue: low expression values, red: high expression values. DKO samples are annotated in red, WT in black, female samples in light grey, and male samples in dark grey. Samples cluster according to genotype but not according to sex. Hierarchical clustering of genes reveals 2 clusters, which contain DEGs either up or downregulated in DKO mice. (E) Log_2 FC of genes coding for voltage-gated sodium (Na^+), chloride (Cl^-), and calcium (Ca^{2+}) channels. Bars are colored in dark grey if the log_2FC was statistically significant.

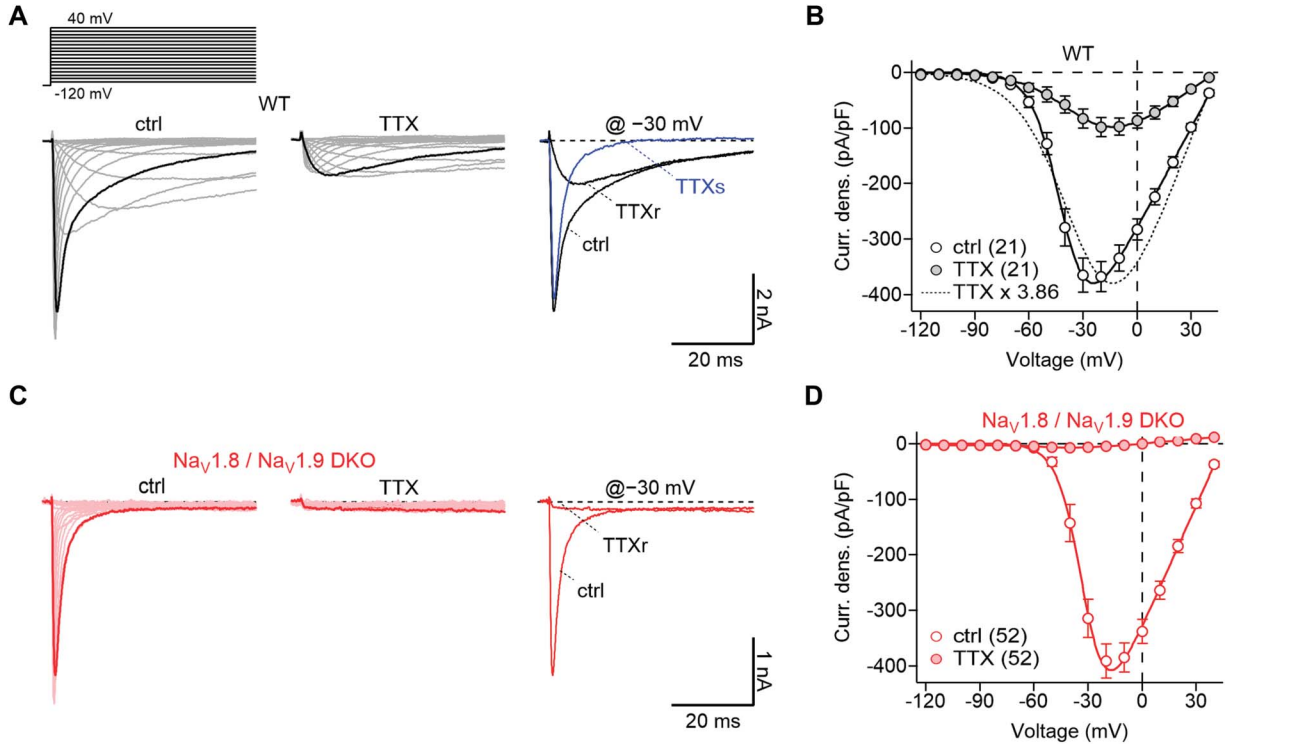

Figure 2. Voltage-dependent activation of total Na^+ currents in wild-type and $Na_V1.8/Na_V1.9$ DKO DRG neurons. (A) Superposition of representative current traces (*bottom*) recorded in a small-diameter wild-type (WT) DRG neuron in response to depolarizations ranging from −120 mV to 40 mV in steps of 10 mV (*top*), before (ctrl) and after (TTX) application of 1 μM TTX. The current traces at −30 mV (thick lines) are shown separately (*right*) to better illustrate the effect of TTX application on fast and slow inactivating current components. The blue trace representing the TTXs current component was obtained by subtracting the response in presence of TTX (TTXr) from the current response under control conditions (ctrl). (B) Mean peak current densities as a function of test pulse voltage, obtained from experiments as shown in *A*. Continuous curves are data fits according to Equation 1. The dotted curve is the fit to the data in presence of 1 μM TTX, scaled in amplitude by a factor of 3.86 to match the peak current density under control conditions. (C and D) Data set as shown in (A and B), recorded in small-diameter $Na_V1.8/Na_V1.9$ DKO DRG neurons. In (D), straight lines connect the data points obtained in the presence of TTX. Data in (B and D) are means ± SEM with the numbers of individual neurons analyzed, *n*, provided in parentheses.

with small amplitudes were evoked, an additional current component with larger amplitude and faster gating kinetics became apparent at higher voltages. Under control conditions, ie, without TTX present in the bath, total Na^+ currents reached a maximum current density of −369 ± 27 pA/pF at −20 mV and activated with a half-maximal voltage (V_m) of −40.5 ± 1.2 mV and an associated slope factor (k_m) reflecting the voltage dependence of activation of 7.3 ± 0.7 mV. Application of 1 μM TTX inhibited specifically the rapidly activating and inactivating current component (TTXs) leading to a reduction of total Na^+ current by 74.0 ± 0.1% (**Figs 2A and B**; Supplementary Fig. 6, http://links.lww.com/PAIN/C139). Analysis of the remaining slow-gating TTXr currents, which are mediated by $Na_V1.8$ and $Na_V1.9$,[70] yielded a V_m value of −30.0 ± 2.8 mV and k_m of 12.6 ± 1.4 mV (both $P < 0.01$; tested against control, ie, before TTX application).

By contrast, $Na_V1.8/Na_V1.9$ DKO neurons gave rise exclusively to fast activating, fast inactivating Na^+ currents in the entire voltage range analyzed (**Fig. 2C**). With −391 ± 31 pA/pF at −20 mV, the mean maximum current density (**Fig. 2D**) was similar to that obtained in wild-type neurons ($P > 0.05$). Voltage-dependent activation of total Na^+ currents in $Na_V1.8/Na_V1.9$ DKO DRG neurons was characterized by a V_m of −30.2 ± 0.9 mV and k_m of 5.8 ± 0.2 mV. Unlike in wild-type neurons, which exhibited a mixture of TTXs and TTXr Na^+ currents, the current responses of $Na_V1.8/Na_V1.9$ DKO neurons ($n = 52$) could be quantitatively inhibited by application of 1 μM TTX (**Figs. 2B and D**, Supplementary Fig. 6, http://links.lww.com/PAIN/C139), confirming the absence of functional $Na_V1.8$ and $Na_V1.9$ channels in these cells and thus the successful double knockout.

As shown in Supplementary Figure 6, http://links.lww.com/PAIN/C139, the time courses of current block by TTX, monitored with repetitive pulses to 0 mV and described with single-exponential functions, were identical in wild-type and $Na_V1.8/Na_V1.9$ DKO neurons, yielding time constants of block (τ_{block}) of 4.6 ± 0.5 seconds and 5.2 ± 0.3 seconds ($P > 0.05$), respectively. Moreover, current responses in both wild-type and $Na_V1.8/Na_V1.9$ DKO neurons recovered completely upon TTX washout, resulting in single-exponential recovery time constants ($\tau_{recovery}$) of 240 ± 21 seconds and 231 ± 24 seconds ($P > 0.05$), respectively.

Total Na^+ currents in wild-type and $Na_V1.8/Na_V1.9$ DKO neurons were further characterized with respect to their voltage-dependent steady-state inactivation (**Fig. 3**). Under control conditions, the voltage dependence of inactivation of Na^+ currents in wild-type neurons displayed 2 components (**Figs. 3A and C**). The major component, which accounted for 73.5 ± 0.5% of total Na^+ currents, was characterized by a half-maximal voltage of inactivation, V_h, of −88.7 ± 1.2 mV and an associated slope factor, k_h, of 6.9 ± 0.6 mV and was sensitive to block by 1 μM TTX (TTXs). The minor component inactivated at more depolarized membrane potentials (V_h: −46.9 ± 1.3 mV, k_h: 5.5 ± 0.3 mV) and was resistant to inhibition by TTX, thus being compatible with $Na_V1.8$ and $Na_V1.9$ as the underlying channels. Steady-state inactivation of Na^+ currents in $Na_V1.8/Na_V1.9$ DKO neurons, which expressed exclusively TTXs currents (**Figs. 3B and D**), was characterized by V_h of −82.2 ± 0.9 mV and k_h of 7.0 ± 0.2 mV largely resembling the inactivation properties of the TTXs current component in wild-type neurons.

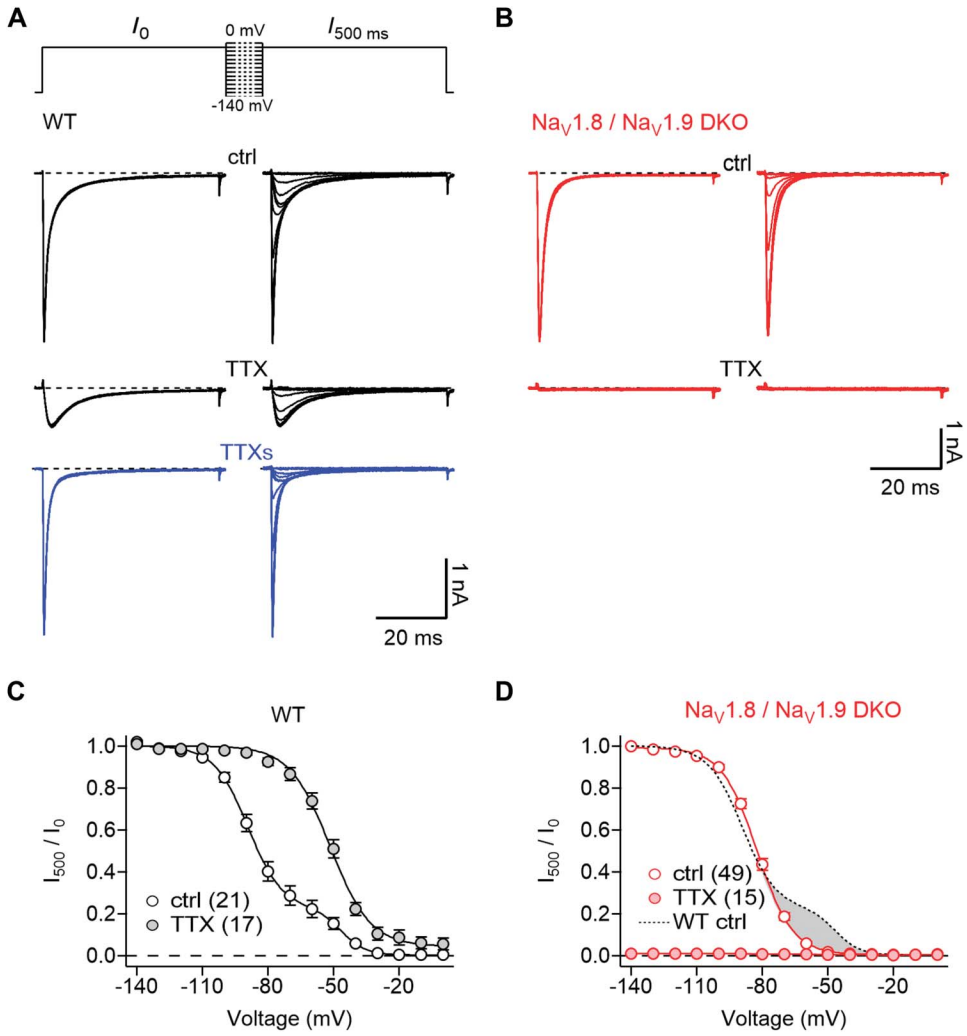

Figure 3. Voltage dependence of steady-state fast inactivation of Na_V channels expressed in WT and $Na_V1.8$/$Na_V1.9$ DKO DRG neurons. (A) Superposition of representative whole-cell current traces obtained from a small-diameter wild-type (WT) DRG neuron at a membrane potential of −10 mV before (I_0) and after (I_{500}) 500-ms conditioning intervals at voltages ranging from −140 mV to 0 mV in steps of 10 mV, in the absence (ctrl) and presence of 1 μM TTX (TTX). The corresponding pulse protocol is shown on top; dashed lines indicate 500-ms conditioning periods. Blue traces representing current components inhibited by application of 1 μM TTX (TTXs) were obtained by subtracting currents in presence of TTX (TTX) from control traces (ctrl). (B) Recordings as shown in *A*, obtained from a small-diameter $Na_V1.8$/$Na_V1.9$ DKO DRG neuron, in the absence (ctrl) or presence (TTX) of 1 μM TTX. (C and D) Normalized steady-state inactivation of Na_V-mediated currents as a function of conditioning voltage in the absence (ctrl) and presence (TTX) of 1 μM TTX, obtained from recordings of WT (C) and $Na_V1.8$/$Na_V1.9$-DKO DRG (D) neurons as shown in *A* and *B*, respectively. Continuous curves are data fits according to Equation 2. In WT neurons (C), Na_V channel inactivation under control conditions displayed 2 components described by a linear combination of parameters characterizing inactivation of TTXs and TTXr channels ($Na_V1.8$- and $Na_V1.9$-mediated TTXr components: 26.5 ± 5.4%). In (D), the data fit characterizing inactivation of Na_V channels in WT neurons under control conditions is superimposed. The gray area in (D) corresponds to $Na_V1.8$- and $Na_V1.9$-dependent currents that are present in WT but not in $Na_V1.8$/$Na_V1.9$ DRG neurons. All data points are mean values ± SEM with the number of experimental replicates, *n*, provided in parentheses.

3.4. The $Na_V1.8$/$Na_V1.9$ double knockout affects the shape of action potentials in dorsal root ganglia neurons

To assess the impact of the double knockout on DRG neuron excitability, whole-cell current-clamp recordings were performed on small-diameter DRG neurons isolated from $Na_V1.8$/$Na_V1.9$ DKO mice and wild-type littermates using bath and pipette solutions closely resembling physiological conditions. After the whole-cell configuration was established in voltage-clamp mode, a brief test pulse to 0 mV was applied from a holding potential of −60 mV, and the resulting current responses were recorded. The neurons generated transient inward currents, mainly reflecting the activity of Na_V channels, overlaid by slower activating, noninactivating outward currents as they are typical for voltage-gated potassium (K_V) channels. Representative recordings obtained from neurons that did not fire spontaneous action potentials in subsequent current-clamp recordings are shown in **Figures 4A and B**. Consistent with the loss of functional $Na_V1.8$ and $Na_V1.9$ channels and the absence of compensatory transcriptional upregulation of other Na_V subtypes (**Fig. 1E**, Supplementary Table 6, http://links.lww.com/PAIN/C139), the inward current densities of DKO neurons was diminished (WT: 254.3 ± 18.6 pA/pF, DKO:, 185.1 ± 24.7, $P < 0.05$), whereas outward current densities remained unaffected (WT: 123.9 ± 9.3 pA/pF, DKO: 120.0 ± 13.3 pA/pF, $P > 0.05$). The cell membrane capacitance (WT: 14.7 ± 0.6 pF, DKO: 13.1 ± 0.6 pF) and the input resistance (WT: 1.50 ± 0.11 MΩ, DKO: 1.78 ± 0.14 GΩ) were also not different between the 2 groups (both $P > 0.05$) (**Fig. 4B**).

As shown in Supplementary Figure 7A, http://links.lww.com/PAIN/C139, after switching to current-clamp mode, spontaneous action potentials occurred in about the same fraction of wild-type and $Na_V1.8$/$Na_V1.9$ DKO cells (WT: 31%, DKO: 26.5%, $P > 0.05$; *z*-test). However, the frequency of spontaneous firing was

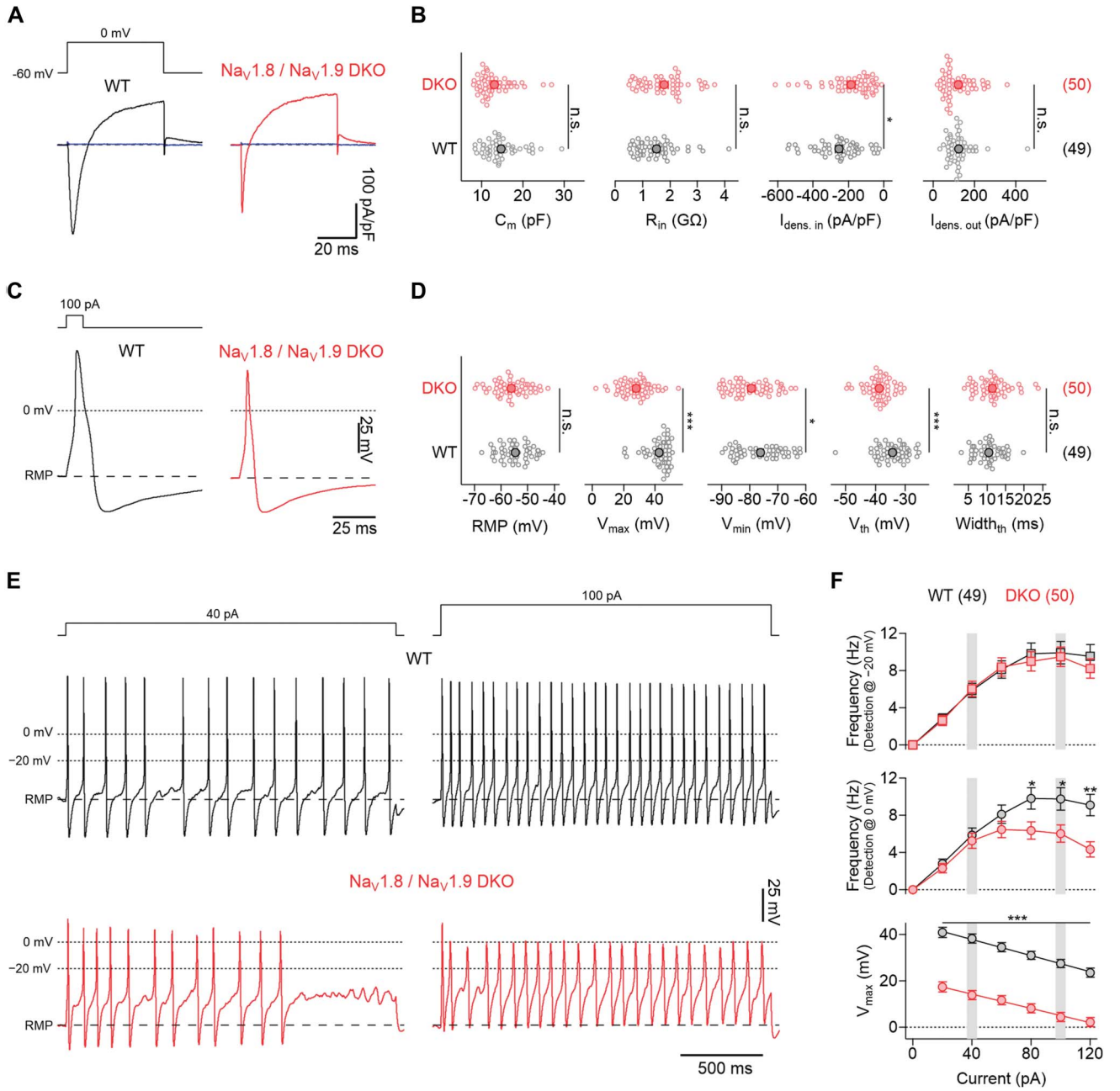

Figure 4. The $Na_V1.8/Na_V1.9$ double knockout reduces the amplitudes of evoked action potentials in DRG neurons but does not affect their firing frequency. (A) Representative whole-cell currents in response to a 50-millisecond-long test pulse to 0 mV, recorded from a small-diameter wild-type (WT, black) or $Na_V1.8/Na_V1.9$ DKO (red) neuron in voltage-clamp mode before proceeding with current-clamp recordings. Blue traces are associated leak currents recorded in response to hyperpolarizing pulses to −69 mV. (B) Parameters obtained from experiments as shown in (A). C_m is the cell membrane capacitance and R_{in} the input resistance. $I_{dens.\ in}$ and $I_{dens.\ out}$ are the inward and outward peak current densities, respectively. (C) Representative single action potentials, elicited in a small-diameter wild-type (WT, black) or $Na_V1.8/Na_V1.9$ DKO (red) neuron in response to a 10-millisecond current injection of 100 pA (*top*). Dotted lines indicate 0 mV; dashed lines mark the level of the RMP. (D) Parameters characterizing action potential properties. RMP: resting membrane potential, V_{max}: maximum action potential voltage, V_{min}: minimum voltage during after-hyperpolarization, V_{th}: action potential voltage threshold, $Width_{th}$: action potential width at V_{th}. (E) Representative trains of action potentials, recorded in a small-diameter wild-type (WT, black) or $Na_V1.8/Na_V1.9$ DKO (red) neuron in response to 2-s current injections of 40 pA (*left*) or 100 pA (*right*). Dotted lines mark 0 mV and −20 mV, both of which served as thresholds for unbiased action potential detection; dashed lines indicate the RMP (WT: −49.1 mV, $Na_V1.8/Na_V1.9$ DKO: −62.3 mV). (F) Action potential firing frequencies using 0 mV (*top*) or −20 mV (*middle*) as detection threshold and averaged action potential peak voltages (V_{max}, *bottom*) obtained from experiments as shown in (E) as a function of injected current. Gray vertical bars mark current injections of 40 pA and 100 pA, which were used to obtain data in (E). Filled symbols in (B, D and F) are means ± SEM with the number of experimental replicates, *n*, provided in parentheses, obtained from a total of 3 animals per genotype. Open symbols in (B and D) represent individual data points. Significance between pairs of data was tested with a 2-sided Student *t*-test: $^{***}P < 0.001$, $^{**}P < 0.01$, $^{*}P < 0.05$, n.s.: not significant.

lower in DKO neurons (2.8 ± 0.7 Hz) compared with wild-type neurons (5.5 ± 1.0 Hz, $P < 0.05$), and the amplitudes of their action potentials also appeared to be lower than in wild-type. Passive membrane properties as well as evoked inward and outward currents were qualitatively similar to that of not spontaneously firing neurons (Supplementary Fig. 7B, http://links.lww.com/PAIN/C139).

To analyze the shape of action potential waveforms, single spikes were evoked in not spontaneously active neurons using 10-ms current injections of 100 pA (**Fig. 4C**). As shown in **Figures 4C and**

D, loss of $Na_V1.8$ and $Na_V1.9$ did not affect the resting membrane potential (RMP; WT: −54.7 ± 0.8 mV, DKO: −56.3 ± 1.1 mV, $P > 0.05$) of DRG neurons nor the duration of evoked spikes ($Width_{th}$; WT: 10.5 ± 0.5 ms, DKO: 11.5 ± 0.8 ms, $P > 0.05$) but significantly reduced the peak amplitude of action potentials by 15 mV (WT: 42.8 ± 1.1 mV, DKO: 27.8 ± 1.8 mV, $P < 0.001$). In addition, in $Na_V1.8/Na_V1.9$ DKO neurons, the minimum voltage during action potential after-hyperpolarization (V_{min}) and the action potential voltage threshold (V_{th}) were decreased by 3.1 mV ($P < 0.05$) and 4.4 mV ($P < 0.001$), respectively.

Firing rates of not spontaneously active neurons were determined by evoking repetitive action potentials with a series of 2-s current injections ranging from 0 to 120 pA in steps of 20 pA. Representative responses of wild-type and DKO DRG neurons to current injections of 40 pA and 100 pA are shown in **Figure 4E**. Because spike amplitudes (V_{max}) were markedly smaller in DKO neurons and tended to fall further at higher stimulation intensities (**Figs. 4E and F**), 2 thresholds, −20 mV and 0 mV, were considered to estimate firing frequencies. Systematic assessment of action potential firing as a function of injected current revealed that firing rates of DKO and wild-type neurons were indistinguishable when the criterion for spike detection was crossing the −20 mV threshold (**Fig. 4F**, *top*). However, increasing the detection threshold to 0 mV reduced the apparent firing frequency of DKO neurons but not that of wild-type neurons at stimulation intensities > 60 pA, demonstrating that in DKO cells a substantial fraction of spikes did not reach the overshooting voltage range as stimulation intensities increased (**Fig. 4F**, *middle*). The averaged amplitudes of evoked repetitive action potentials analyzed as a function of injected current further revealed that spike amplitudes decayed linearly in both wild-type and DKO DRG neurons with similar stimulation intensity dependencies of 3.5 mV (WT) and 3.1 mV (DKO) per 20 pA of injected current (**Fig. 4F**, *bottom*).

To determine the impact of the RMP on evoked repetitive firing, firing frequencies and RMPs of all neurons analyzed were visualized in scatter plots, and the slopes obtained from linear data fits were used to qualitatively assess the relation between action potential firing frequency and RMP (Supplementary Fig. 8, http://links.lww.com/PAIN/C139). In wild-type neurons, a high RMP favored high firing frequencies especially at low stimulation intensities (<60 pA), as indicated by positive slopes of the associated regression lines. This correlation gradually reversed as stimulation intensities increased, with high firing frequencies then (>80 pA) being observed more frequently in neurons with a comparably low RMP. This relationship between evoked firing behavior and RMP was qualitatively similar in DKO DRG neurons (Supplementary Fig. 8, http://links.lww.com/PAIN/C139). In these cells, a higher RMP was also associated with higher firing frequencies, but compared to wild-type neurons, this correlation was more pronounced and also evident at higher stimulation intensities up to and including 80 pA.

Collectively, the data show that the combined loss of $Na_V1.8$ and $Na_V1.9$ affects the shape but not the firing frequency of action potentials in DRG neurons.

3.5. $Na_V1.8/Na_V1.9$ double knockout mice show changes in C-fiber dorsal root ganglia neuron populations and moderate signs of peripheral axonal degeneration

Because $Na_V1.8$ and $Na_V1.9$ are coexpressed in a substantial proportion of C-fiber nociceptors, we analyzed the effects of the $Na_V1.8/Na_V1.9$ double knockout on C-fiber neuron survival and DRG/sciatic nerve anatomy. Using fluorescently labelled isolectin-B4 (IB4) and Plexin C1 (PlxnC1) antibodies to visualize unmyelinated nonpeptidergic (NP1-3) and a fraction of peptidergic C-nociceptors (PEP1)[74] together with the pan-sensory neuron marker PGP9.5 in DRG sections (**Fig. 5A**), we did not observe changes in these C-nociceptors in number and distribution in $Na_V1.8/Na_V1.9$ deficient mice. In line with these data, flow cytometry analysis of $IB4^+$ and $CGRP^+$ C-nociceptor subtypes in dissociated DRGs of 2-month-old WT and $Na_V1.8/Na_V1.9$ DKO mice revealed no changes in relative numbers of $IB4^+$ and $CGRP^+$ C-nociceptors (Supplementary Fig. 5A,B, http://links.lww.com/PAIN/C139). Interestingly, while the total number of neurons decreased with age (12- to 18-month-old mice, Supplementary Fig. 5C, http://links.lww.com/PAIN/C139), the relative fraction of $IB4^+$ and $CGRP^+$ C-nociceptors remained constant suggesting no age-related C-fiber specific neurodegeneration in DKO DRGs (Supplementary Fig. 5D, http://links.lww.com/PAIN/C139). Centrally, $IB4^+$ afferent C-fibers terminate in spinal cord dorsal horn laminae IIo/IIi adjacent to $CGRP^+$ fibers, and we found this projection pattern not disturbed in $Na_V1.8/Na_V1.9$ DKO dorsal spinal cord (**Fig. 5B**). However, consistent with the downregulation of TH/C-LTMR marker genes (**Figs. 1C and D**), TH immunoreactivity was strongly decreased in DKO compared to WT DRG sections suggesting a loss or functional impairment of this C-fiber subtype (**Fig. 5C**).

In addition, we performed electron microscopy on DRG, sciatic nerve, and skin tissues of mice 34 to 52 weeks old (**Fig. 6**). We first examined semithin sections of WT and $Na_V1.8/Na_V1.9$ DKO DRGs, which did not reveal any obvious anatomical changes (**Figs. 6A and B**). Using higher-magnification electron micrographs, we observed, compared to WT sciatic nerve tissue (**Fig. 6C**), several aspects of moderate axon degeneration in DKO sciatic nerve (**Figs. 6D–H**). While myelinated nerve fibers in DKO sciatic nerve appeared largely normal, Remak bundles comprising unmyelinated fibers contained both normal and swollen axons (**Fig. 6E**), collagen pockets (**Fig. 6F**), and degenerating axons with reduced diameter (**Fig. 6G**). In addition, Schwann cell morphology was also impaired in the DKO tissue, as indicated by enlarged endoplasmic reticulum (ER) profiles, autophagic deposits, and basal lamina onion bulbs (**Fig. 6H**). In contrast, glabrous skin dermal nerve fascicles of WT (**Fig. 6I**) and $Na_V1.8/Na_V1.9$ DKO (**Figs. 6J and K**) animals were normal except for few swollen degenerating axons (**Fig. 6K**).

Taken together, the $Na_V1.8/Na_V1.9$ DKO caused detectable alterations in the ultrastructure of sensory neurons and their surrounding tissue, compatible with a mild peripheral neuropathy.

3.6. $Na_V1.8/Na_V1.9$ double knockout mice have a significantly higher noxious mechanical threshold

To investigate the impact of $Na_V1.8$ and $Na_V1.9$ deletion on pain thresholds, a series of behavioral tests were performed across different pain modalities in 8- to 16-week-old WT and DKO mice. Mechanical sensitivity to innocuous stimuli was assessed using the up-down von Frey test on the hind paw. No differences were observed between the WT and DKO groups (**Fig. 7A**). However, sensitivity to noxious mechanical stimuli such as the Randall–Selitto test on the tail was significantly different between the groups (**Fig. 7B**): DKO mice had on average a significantly higher noxious mechanical threshold (124 ± 30 g for WT and 254 ± 81 g for DKO, $P < 0.0001$, unpaired *t* test), which is in line with previous studies showing increased thresholds to noxious mechanical pressure stimuli for mice deficient for either $Na_V1.8$ or $Na_V1.9$.[3,46]

3.7. $Na_V1.8/Na_V1.9$ double knockout mice do not show altered thresholds to cold or heat

A set of behavior tests were performed to assess heat (**Figs. 7C and D**) and cold (**Figs. 7E–H**) thresholds. Behavior tests

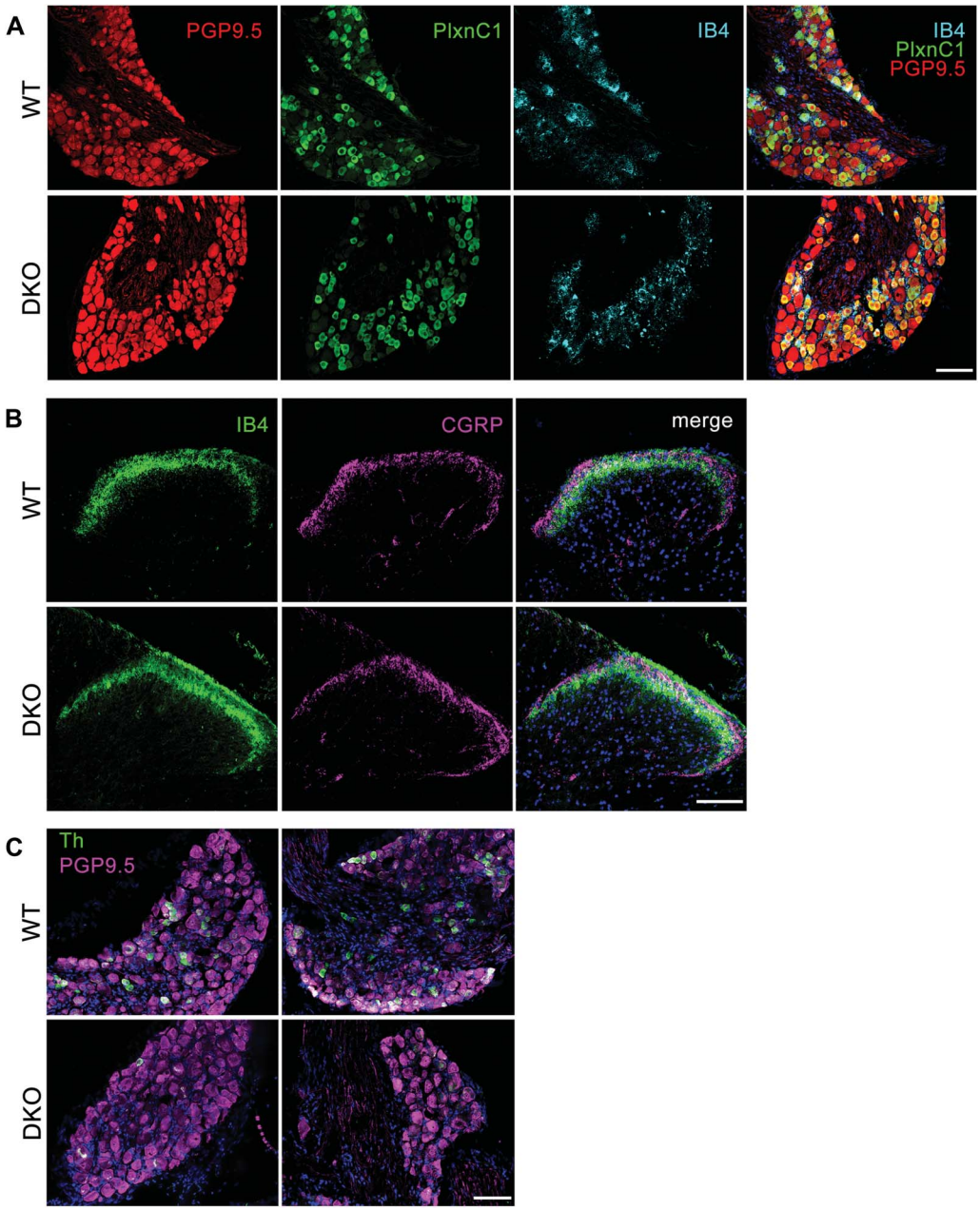

Figure 5. $Na_V1.8/Na_V1.9$ DKO alters marker profile of DRG C-fiber subpopulations. (A) Immunofluorescence staining of DRG sections with markers for nonpeptidergic unmyelinated C-fiber nociceptors (PlxnC1, green; IB4, cyan). Note, a fraction of $PlxnC1^+$ neurons are also positive for IB4. Pan-neuronal marker: PGP9.5 (red). (B) Spinal cord sections stained for IB4 (green; nonpeptidergic, unmyelinated C-nociceptors) and CGRP (magenta; peptidergic, unmyelinated C-nociceptors) indicate no change in the pattern of dorsal horn projections for these DRG neuron subpopulations. (C) Reduction in Th immunosignals suggests a loss of C-LTMR neurons in $Na_V1.8/Na_V1.9$ DKO mice (Th, green; PGP9.5, magenta). $n = 2$ animals per genotype. Nuclei in (A–C) are stained in blue (DAPI), scale bars: 100 μm (A and B), 50 μm (C).

assessing cold included a cold plate at 5°C for 1 min/10°C for 10 minutes where the time spent with the forepaws lifted was counted, nocifensive responses to the cooling effect of a droplet of acetone application to the hind paw, and latency to the hind paw withdrawal to dry ice application through a glass platform. Thresholds to cold sensitivity were not significantly different between WT and DKO mice (**Figs. 7E–H**). Furthermore, heat thresholds to noxious heat as determined by the latency to the first nocifensive response in a 55°C hot plate test (**Fig. 7C**) and by the latency in the Hargreaves test, measuring thermal spinal reflex, were similar between the groups (**Fig. 7D**). In addition, thermal place preference tests were run with 3 different conditions (10°C vs 0°C, 20°C vs 10°C, and 30°C vs 5°C, **Figs. 8A–C**). No differences were observed between genotypes for all temperature combinations tested; however, for 30°C vs 5°C place preference $Na_V1.8/Na_V1.9$ DKO mice tended to spend more time on the 5°C plate, but this tendency did not reach the level of significance ($P = 0.19$, **Fig. 8C**).

3.8. $Na_V1.8/Na_V1.9$ deletion does not affect formalin-induced nocifensive behavior

To assess the role of $Na_V1.8$ and $Na_V1.9$ deletion in acute inflammation, the formalin test (5%) was performed. No differences were seen in $Na_V1.8/Na_V1.9$ DKO mice nocifensive responses during the 60-min observation period compared to

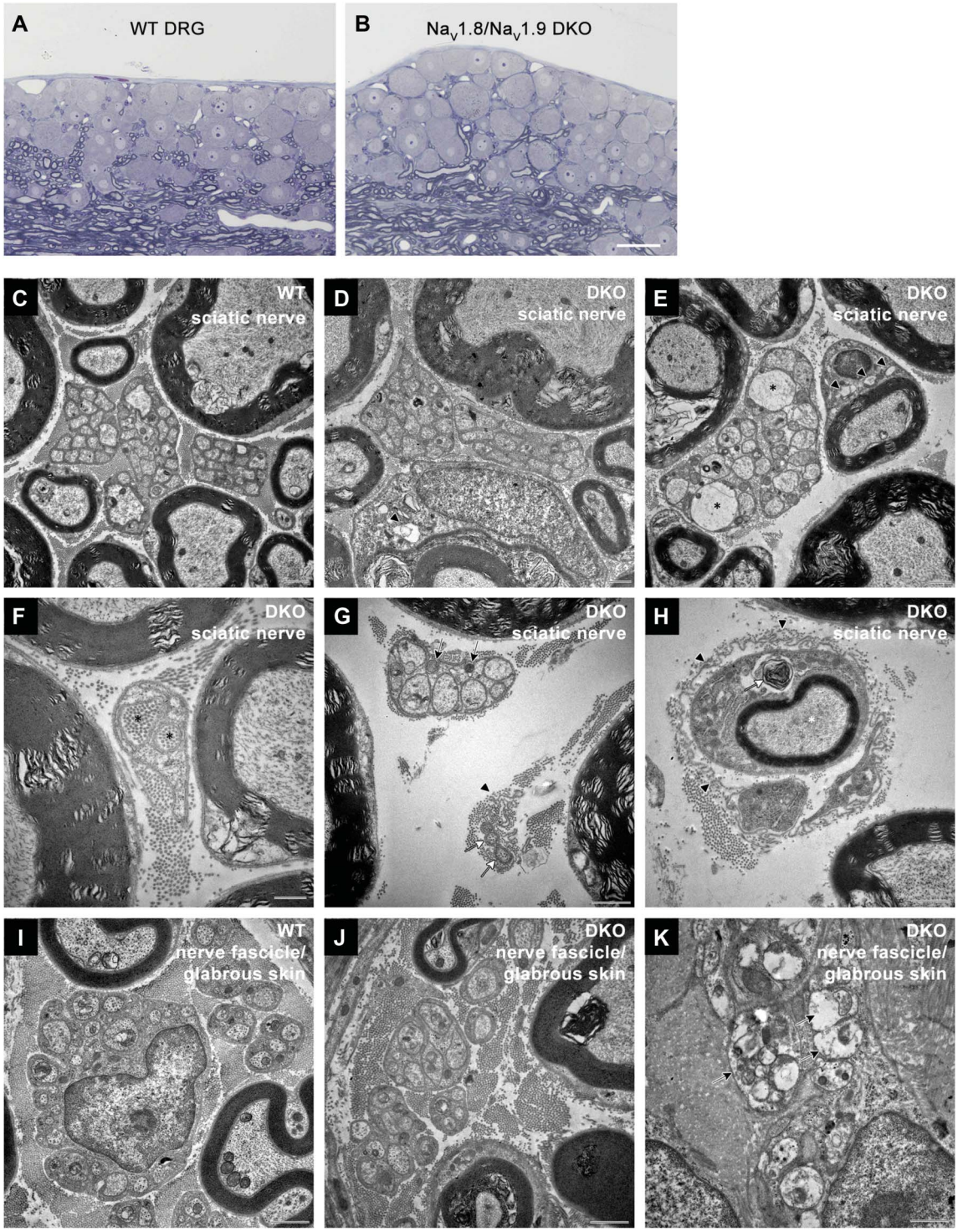

Figure 6. Ultrastructural abnormalities in $Na_V1.8/Na_V1.9$ DKO mice indicate moderate peripheral axonal degeneration. (A and B) Electron micrographs of representative semithin sections of WT (A) and $Na_V1.8/Na_V1.9$ DKO (B) DRGs. Both samples show a number of neurons and myelinated axons without discernible pathological alterations. No noticeable reduction of neuron numbers in DKO animals compared to WT. Scale bar: 50 μm. (C) Wild-type (WT) sciatic nerve with multiple myelinated axons presenting normal myelin thickness and 3 Remak bundles with several unmyelinated nerve fibers of different diameters. (D) $Na_V1.8/Na_V1.9$ DKO (DKO) sciatic nerve with largely normal myelinated nerve fibers and 2 Remak bundles with many, mostly small-diameter unmyelinated axons. A myelinating Schwann cell shows widened ER profiles (arrowhead) as sign of ER stress. (E) DKO sciatic nerve with a Remak bundle containing normal, as well as swollen unmyelinated axons (asterisks). Again, the myelinating Schwann cell shows enlarged ER vesicles (arrowheads). (F) DKO sciatic nerve shows an empty Remak bundle with 2 collagen pockets (asterisks) indicating loss of unmyelinated fibers. (G) DKO sciatic nerve with a Remak bundle exhibiting several normal diameter axons and a few very small, possibly degenerating ones (arrows). Arrowheads show remnants of basal lamina with only a few Schwann cell profiles (white arrows). (H) Basal lamina onion bulb with redundant basal lamina (arrowheads), a remyelinated axon (asterisk) with disproportionately thin myelin and autophagic material in the Schwann cell cytoplasm (white arrow), most likely myelin debris. (I) Dermal nerve fascicle from WT glabrous skin with normal myelinated axons and a Remak bundle with many, mostly small-diameter axons. (J) A dermal nerve fascicle from DKO glabrous skin shows largely normal myelinated and unmyelinated axons, and (K) only in a few instances swollen degenerating axons could be found (arrows). Number of mice analyzed: $n = 3$ WT, $n = 3$ DKO. Scale bars: (F): 0.5 μm, all others: 1 μm.

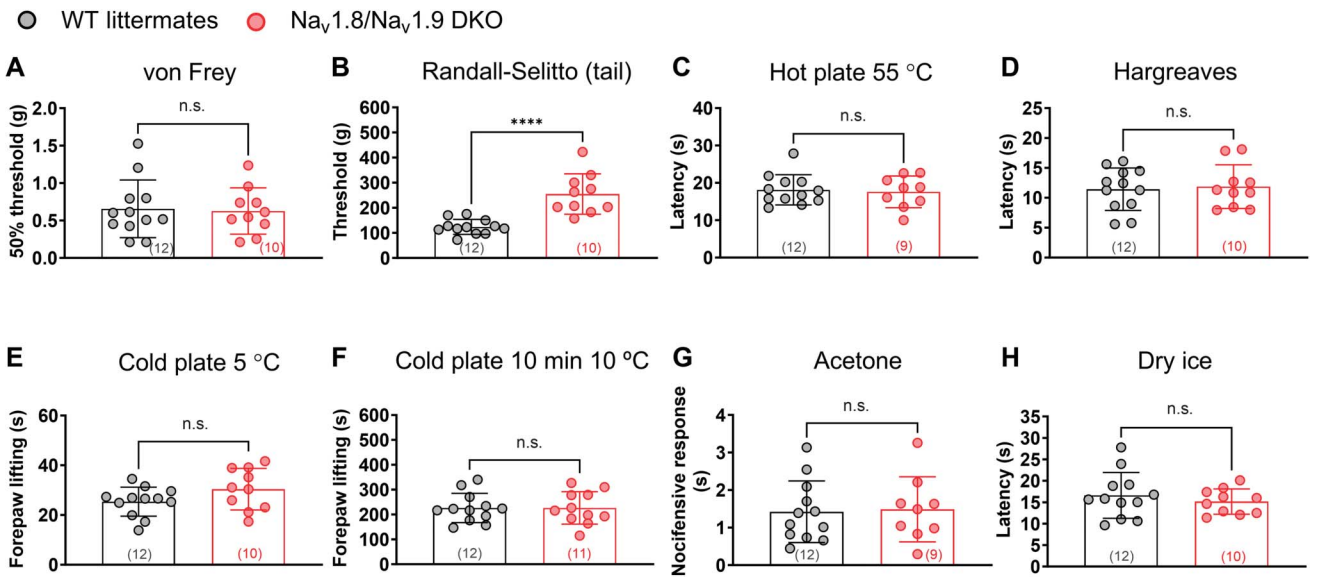

Figure 7. $Na_V1.8/Na_V1.9$ DKO mice show altered noxious mechanical pressure threshold but no changes in heat or cold thresholds. (A) The 50% withdrawal threshold to stimulation with von Frey hairs was not different between WT and $Na_V1.8/Na_V1.9$ DKO mice. (B) $Na_V1.8/Na_V1.9$ DKO mice showed increased threshold to noxious mechanical stimulation compared to WT mice. $^{****}P < 0.0001$. (C) The latency to the first hind paw lick or jump was measured. This was not significantly different between WT littermates and $Na_V1.8/Na_V1.9$ DKO mice. (D) Latency to paw withdrawal was not significantly different in the Hargreaves test between WT littermates and $Na_V1.8/Na_V1.9$ DKO mice. (E) Time spent with forepaws lifted on a 5°C cold plate during a total of 60 seconds for WT littermates and $Na_V1.8/Na_V1.9$ DKO mice. (F) Time spent with forepaws lifted on a 10°C cold plate for a total of 10 minutes for WT littermates and $Na_V1.8/Na_V1.9$ DKO mice. (G) Nocifensive responses to the cooling effect of acetone on the hind paw within the first minute postapplication was not significantly different between the groups. (H) Mice were placed on a glass stand in individual Perspex boxes. A tube containing dry ice was applied below the hind paw and the latency to the first response was measured for WT littermates and $Na_V1.8/Na_V1.9$ DKO mice. Error bars in (A-H) represent mean ± SD with the number of animals used per group provided in parentheses. Statistical indicators refer to an unpaired two-sided Student *t*-test: $^{****}P < 0.0001$; n.s., not significant.

WT mice (**Fig. 8D**). In addition, the total time spent licking/flinching/biting the injected paw, pooled to phase I and phase II of the formalin test, was not significantly different either (**Fig. 8E**), in line with previous results suggesting a dominant role of $Na_V1.7$ in nocifensive responses to intraplantar formalin injection.[51]

3.9. Double knockout dorsal root ganglia neurons facilitate expression and functional analysis of heterologous $Na_V1.8$ and $Na_V1.9$ channels

$Na_V1.8$ and $Na_V1.9$ channels are important regulators of DRG neuron excitability, and mutations in the corresponding human genes *SCN10A* and *SCN11A* give rise to a wide spectrum of pain disorders ranging from congenital analgesia to chronic neuropathic pain conditions.[8] The functional analysis of the human isoforms of $Na_V1.8$ and $Na_V1.9$ and associated pathological variants in a DRG neuron background is, therefore, particularly desirable. However, assessment of the gating properties of overexpressed $Na_V1.8$ and $Na_V1.9$ variants in murine WT DRG neurons or DRG neurons obtained from mice lacking either $Na_V1.8$ or $Na_V1.9$ is compromised by the overlapping expression of TTXr $Na_V1.8$ and/or $Na_V1.9$ channels endogenous in these cells. Because $Na_V1.8/Na_V1.9$ DKO neurons do not express interfering endogenous TTXr Na_V channels (**Figs. 2 and 3**), they are expected to substantially facilitate the functional profiling of exogenous $Na_V1.8$ and $Na_V1.9$ variants in voltage-clamp experiments. We, therefore, expressed human $Na_V1.8$, $Na_V1.9$, and the congenital analgesia–associated variant $Na_V1.9$-L811P described previously[37] in isolated $Na_V1.8/Na_V1.9$ DKO DRG neurons using electroporation-mediated plasmid delivery and then analyzed the properties of the channels in whole-cell voltage-clamp experiments. To isolate the current responses of overexpressed channels, all recordings were performed with 1 μM TTX present in the bath solution, assuring quantitative inhibition of endogenous TTXs Na^+ currents. Voltage-dependent activation and inactivation characteristics of the human channels were analyzed by applying the same test pulse paradigms as used in **Figures 2 and 3**, respectively.

As demonstrated in **Figures 9A and B**, human $Na_V1.8$ channels gave rise to fast activating, slow inactivating currents typical for this Na_V subtype. Mean inward current densities of $hNa_V1.8$ reached a maximum of −190 ± 35 pA/pF at a test pulse voltage of −10 mV; the half-maximal voltage for channel activation (V_m) was −20.9 ± 1.7 mV, and the corresponding slope factor (k_m) was 8.4 ± 0.9 mV. Voltage-dependent inactivation in response to 500-millisecond conditioning periods was described by a half-maximal voltage of inactivation (V_h) of −47.0 ± 1.9 mV and a slope factor (k_h) of 6.4 ± 0.4 mV.

As shown in **Figures 9C and D**, human $Na_V1.9$ and $Na_V1.9$-L811P channels were also functional in DKO neurons, yielding similar mean peak current densities of −125 ± 24 pA/pF at −30 mV and −149 ± 29 pA/pF at −50 mV, respectively. Analysis of peak current densities as a function of test pulse voltage (**Fig. 9E**) revealed that mutation p.L811P caused a shift of the half-maximal voltage of channel activation by −20 mV (WT: −52.8 ± 1.3 mV, p.L811P: −73.0 ± 3.0 mV, $P < 0.001$) without affecting the associated slope factor (WT: 7.7 ± 0.6 mV, p.L811P: −7.5 ± 0.7 mV, $P > 0.05$) (**Fig. 9E**). In addition, the mutation did not significantly affect V_h (WT: −63.6 ± 1.6 mV, p.L811P: −66.4 ± 5.4 mV, $P > 0.05$) but increased k_h from 9.6 ± 0.5 mV to 16.3 ± 0.9 mV (**Fig. 9F**). The differences in the gating of $Na_V1.9$ wild-type and p.L811P mutant channels expressed in $Na_V1.8/Na_V1.9$ DKO-DRG neurons are qualitatively similar to those observed in a previous study in which the functional parameters of both channel variants were examined in transfected ND7/23 cells.[37]

In summary, the data show that $Na_V1.8/Na_V1.9$ DKO-DRG neurons provide a valuable resource that facilitates

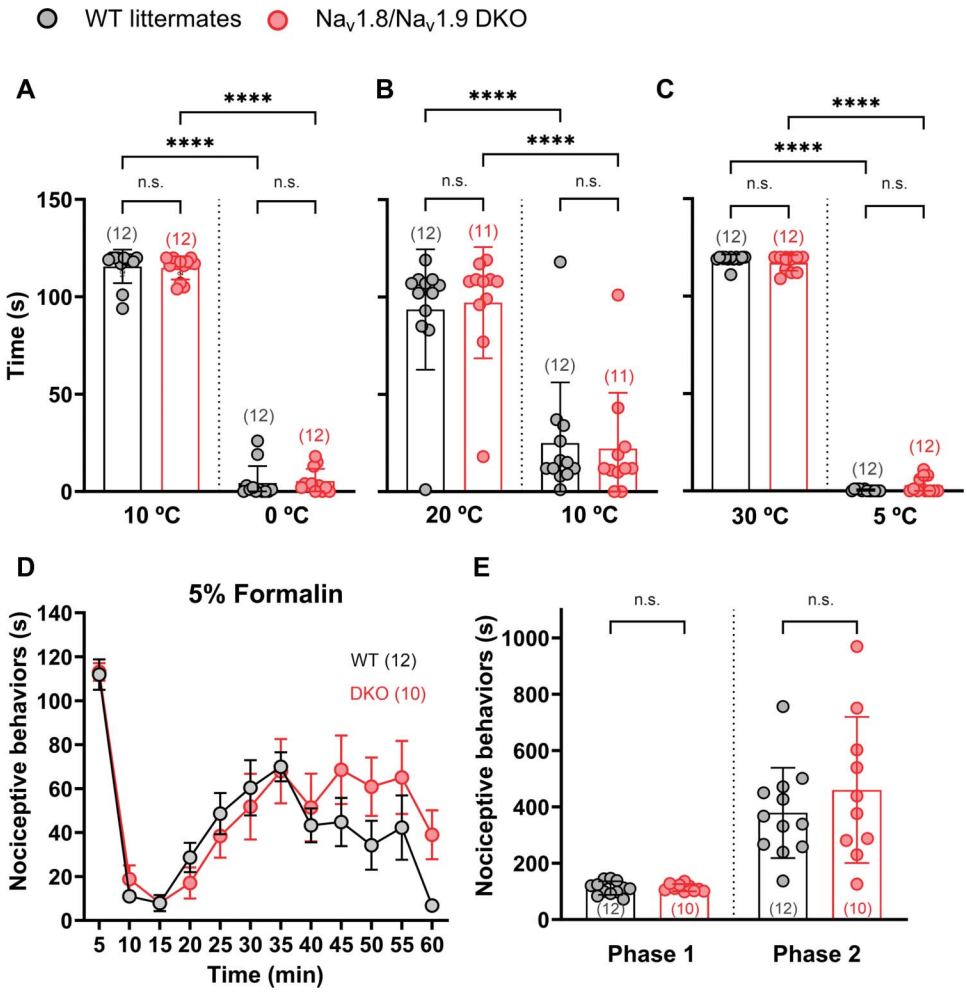

Figure 8. Na$_V$1.8/Na$_V$1.9 DKO mice show neither thermal place preference to cold nor reduced formalin-induced nocifensive behavior. Na$_V$1.8/Na$_V$1.9 DKO mice and WT littermates were placed in a chamber with 2 plates at 10°C and 0°C (A), 20°C and 10°C (B), or 30°C and 5°C (C). The time spent on each plate was measured. No differences were observed between the groups for each time spent in each temperature. No differences were seen in the total number of crossings between plates for each temperature combination (data not shown). (D) After intraplantar injection of 5% formalin, the time spent licking/biting/flinching the injected paw was quantified for Na$_V$1.8/Na$_V$1.9 DKO mice and WT littermates. Groups were not significantly different across time. (E) Nociceptive behaviors for phase I (0-5 min) and phase II (10-60 minutes) of the formalin test. Data were not significantly different. No differences were seen between males and females (data not shown), so the data are pooled together (A–E). Data are presented as mean ± S.D. except (E) which is presented as mean ± SEM. The number of animals used per group is shown in parentheses. Statistical significance between groups was tested using one- (A-C, E) or 2-way (D) ANOVA with Šidák multicomparison test.

structure–function studies of human Na$_V$1.8 and especially Na$_V$1.9 channels, whose functional heterologous expression is notoriously difficult.[75,80]

4. Discussion

Na$_V$1.8 and Na$_V$1.9 channels exhibit complex yet largely overlapping expression patterns in small-diameter DRG neurons,[5,8] most of which give rise to nociceptive C-fibers. The impact of a codeletion of both channels had not been investigated because *Scn10a* and *Scn11a* are genetically linked, preventing the generation of DKO mice by mating Na$_V$1.8 and Na$_V$1.9 single KO animals.

Here, we generated a mouse line lacking Nav1.8 and Nav1.9 using CRISPR/Cas9-gene editing. The success of the strategy was confirmed by RT-PCR and deep sequencing without evidence for off-targets. In addition, whole-cell voltage-clamp recordings on isolated DKO DRG neurons confirmed the KO on the functional level. Application of 1 μM TTX during recordings quantitatively inhibited Na^+ currents in DKO DRG neurons, demonstrating that Na$_V$1.8 and Na$_V$1.9, the predominant TTXr subtypes in DRG neurons,[5] were successfully eliminated. Previous studies have shown that adult rat DRG neurons express low levels of a third TTXr Na$_V$ subtype in addition to Na$_V$1.8 and Na$_V$1.9,[59] compatible with the presence of Na$_V$1.5.[58] Low levels of Na$_V$1.5 mRNA (*Scn5a*) have been detected in subsets of mouse DRG neurons as demonstrated previously[74] and shown here. Consistent with these findings and the significant downregulation of *Scn5a* (**Fig. 1E**, Supplementary Table 6, http://links.lww.com/PAIN/C139), we did not detect TTXr Na^+ currents in DKO DRGs. Furthermore, mRNA expression levels of other Na$_V$ subtypes were found unchanged. This contrasts with previous studies on Na$_V$1.8 or Na$_V$1.9 KO mice. For example, voltage-clamp recordings performed on Na$_V$1.8 KO DRG neurons revealed increased Na^+ currents mediated by unspecified TTXs Na$_V$ subtypes.[3] Furthermore, mRNAs of Na$_V$1.8 and TTXs subtypes (Na$_V$1.1-1.3 and Na$_V$1.7) were found moderately increased in Na$_V$1.9 KO DRG neurons.[56]

However, Na$_V$ channel–mediated current densities were comparable in WT and DKO DRG neurons (**Fig. 2**). A possible, albeit speculative, explanation could be that the increased activity of TTXs Na$_V$ channels in DKO neurons is a consequence of altered post-translational regulatory mechanisms. On the other hand, in recordings performed under more physiological

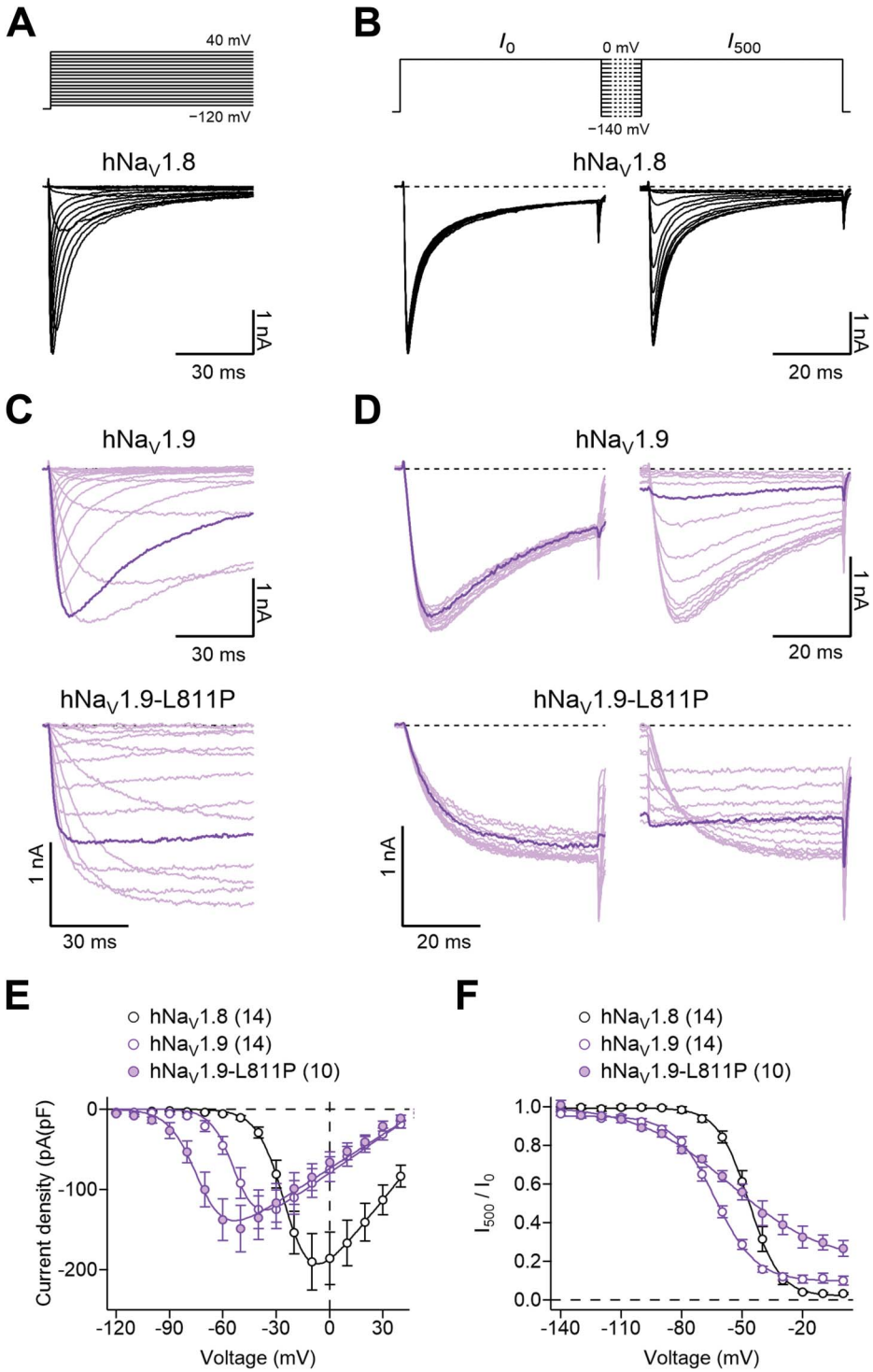

Figure 9. $Na_V1.8/Na_V1.9$ DKO DRG neurons facilitate expression and functional analysis of human $Na_V1.8$ and $Na_V1.9$ channels. (A) Superposition of representative current traces (*bottom*) of $hNa_V1.8$ channels expressed in a $Na_V1.8/Na_V1.9$ DKO DRG neuron in response to depolarizations ranging from −120 mV to 40 mV (*top*). (B) Current traces (*bottom*) obtained from the same neuron as shown in *A*, in response to 50-millisecond depolarizations at −10 mV applied before (I_0) and after (I_{500}) conditioning of the cell for 500 ms at voltages ranging from −140 mV to 0 mV in steps of 10 mV (*top*). (C–D) Experiments as shown in *A* and *B* with neurons expressing either $hNa_V1.9$ (*top*) or $hNa_V1.9$-L811P channels (*bottom*). In (D), test pulses to −40 mV and −60 mV were used to activate $hNa_V1.9$ and $hNa_V1.9$-L811P channels, respectively. To facilitate comparison of $hNa_V1.9$ and $hNa_V1.9$-L811P channels, responses to −30 mV (C) and −50 mV (D) are highlighted. (E) Peak current densities of $hNa_V1.8$, $hNa_V1.9$, and $hNa_V1.9$-L811P channels upon expression in $Na_V1.8/Na_V1.9$ DKO DRG neurons as a function of test pulse voltage, obtained from experiments as shown in (A and C). Continuous curves are data fits according to Equation 1. (F) Voltage dependence of steady-state fast inactivation of $hNa_V1.8$, $hNa_V1.9$, and $hNa_V1.9$-L811P channels obtained from experiments as shown in (B and D), with superimposed data fits according to Equation 2. Data points in *E* and *F* are means ± SEM with *n* provided in parentheses. All data were obtained in the presence of 1 μM TTX.

conditions, DKO DRG neurons yielded smaller inward currents (**Figs. 4A and B**), most of which are mediated by Na_V channels, which is in good agreement with the RNAseq data.

As revealed by current-clamp recordings, small-diameter WT and DKO DRG neurons also differed considerably with respect to their action potential characteristics. Most action potentials

evoked in DKO DRG neurons exhibited an unphysiological morphology characterized by reduced peak voltage, hyperpolarized action potential voltage threshold, and decreased voltage minimum during after-hyperpolarization. In response to sustained depolarizing current injections, action potential peak voltages decreased further as stimulation intensities increased, resulting in a significant proportion of nonovershooting and, thus, physiologically less effective action potentials in DKO DRG neurons. The impairment of action potential electrogenesis in DKO DRG neurons is reminiscent of the situation in $Na_V1.8$-deficient DRG neurons, which exhibit similar action potential properties.[57,60] As shown in an in silico study[25] and by current-clamp recordings on $Na_V1.9$-KO DRG neurons,[37,56] $Na_V1.9$ channels, unlike $Na_V1.8$, contribute little to the fast upstroke of the action potential in DRG neurons nor does their knockout induce major alterations to the shape of action potential waveforms. Therefore, the lack of $Na_V1.8$ is most likely responsible for the altered electrophysiological properties of DKO DRG neurons.

We further found evidence of moderate chronic degeneration of unmyelinated axons and Schwann cells in the sciatic nerve of $Na_V1.8$/$Na_V1.9$ DKO mice. In contrast, nerve fascicles in glabrous skin and intact DRG ganglia, which contain the somata of primary afferents, showed no apparent abnormalities. Because immunostainings on DRG sections and FACS analysis of dissociated DRG neurons showed neither affected absolute and relative numbers of peptidergic and nonpeptidergic unmyelinated neurons nor their distribution within ganglia, the observed axonal degeneration could well be in alignment with a selective loss of C-LTMR neurons whose axonal endings mainly innervate hairy skin.[39]

Although DKO animals showed signs of damage in peripheral afferents and marked deficits in DRG action potential genesis, their responses to acute pain stimuli such as formalin, heat, cold, and innocuous mechanical pressure were indistinguishable from those of WT littermates. The innocuous mechanical and heat thresholds remained unchanged in DKO mice, which is in agreement with the extensive literature on single Na_V KO mice (**Table 1**).[3,38,51,56] Thus, for these sensory modalities, no synergetic effects of the double deletion were evident. However, the threshold to noxious mechanical stimuli (here, sacral spinal levels) was significantly increased in $Na_V1.8$/$Na_V1.9$ DKO mice. Previous studies using $Na_V1.8$ and $Na_V1.9$ single KOs also reported an increase in the noxious mechanical threshold[3,51] in response to the Randall–Selitto test applied on the tail.[46] Yet, double deletion did not completely abolish noxious mechanical sensation on the tail, as only one $Na_V1.8$/$Na_V1.9$ DKO mouse reached the cutoff weight.

Interestingly, although single deletion of $Na_V1.8$ or $Na_V1.9$ has been linked to altered cold thresholds,[43,81] we did not observe changes in cold thresholds of DKO mice. Importantly, most studies describing altered cold sensitivity used in vitro models and cold stimuli applied directly to the somata of DRG neurons. However, increasing evidence indicates no changes in $Na_V1.8$ KO in vivo thresholds to cold stimuli in acute experiments, except for prolonged noxious cold.[44] Here, we found no differences in vivo in cold sensation as measured by cold-plate test (5 and 10°C), acetone application, and dry ice application. Previous reports have also linked $Na_V1.8$ and $Na_V1.9$ KO with increased cold preference.[43,48] However, $Na_V1.8$/$Na_V1.9$ DKO mice, like their WT littermates, showed a preference for the warmest plate under all conditions tested.

To further investigate pain processing, we performed the formalin test. Surprisingly, no significant differences in nocifensive behaviors were seen in DKO mice. This test has been previously reported in $Na_V1.7$, $Na_V1.8$, and Nav1.9 KO studies.[51,52,56] While $Na_V1.7$ deletion resulted in a significant reduction in nocifensive behaviors, $Na_V1.8$ KO studies have shown no impact, and $Na_V1.9$ KO studies have shown a reduction in the second phase, yet of variable statistical significance across different research groups.[38,42,56] Furthermore, diphtheria toxin fragment A (DTA)-mediated ablation of $Na_V1.8$-expressing neurons, many of which also express $Na_V1.9$,[74] dramatically reduced the second phase of the formalin test.[1] Thus, our formalin data show that deleting $Na_V1.8$ and $Na_V1.9$ is not sufficient to achieve $Na_V1.8$Cre DTA ablation levels, suggesting another element integral to $Na_V1.8$-expressing neurons is key in this reduction.

Because the acute pain behavior of the DKO mice is overall only moderately impaired despite considerable functional deficits of their DRG neurons, one could assume compensatory mechanisms that involve the remodeling of circuits downstream of the DRG neurons.

Our mRNA analysis revealed downregulation of canonical C-LTMR marker genes (*Th*, *Slc17a8*, *Tafa4*, *Caecam10*, *Kcnj6*) as well as downregulation of other genes expressed in or associated with this neuron subpopulation (*Exoc1l*, *C1ql4*, *Wfdc2*, *Pou4f2*, *Nxpe2*, *Celf3*, *Gpx2*, *Fbp2*).[22,33,64,67,71,76] Together with the reduced Th immunoreactivity observed in DKO DRGs, this suggests a loss or dysfunction of C-LTMRs in $Na_V1.8$/$Na_V1.9$ DKO animals. C-LTMRs mediate pleasant touch[39,41] and itch sensation[61] but are also known modulators of pain perception.[55] Such a modulatory mechanism is expected to occur predominantly at the level of postsynaptic circuits in the dorsal spinal cord, where C-LTMR input modulates the firing frequency of inhibitory and excitatory interneurons.[78] Interestingly, activity-dependent changes in gene expression after postnatal $Na_V1.7$ removal have been reported to specifically occur in C-LTMRs and are accompanied by C-LTMR-exclusive *Penk* upregulation.[19] By contrast, we observed *Penk* upregulation in $Na_V1.8$/$Na_V1.9$-DKO DRGs despite a putative dysfunction or loss of C-LTMRs, suggesting that gene regulatory mechanisms are differentially affected in $Na_V1.7$-single and $Na_V1.8$/$Na_V1.9$-DKO DRGs. However, given the large number of deregulated genes in DKO DRGs, more specific analyses are needed to determine their individual roles in nociception and if and how their individual or combined deregulation contributes to the overall mild phenotype of the animals.

In addition, we demonstrated that human $Na_V1.8$ and $Na_V1.9$ channels can be successfully overexpressed in DKO DRG neurons and functionally analyzed using the whole-cell voltage-clamp technique. Heterologous expression of human $Na_V1.8$ and $Na_V1.9$ yielded robust $Na_V1.8$- and $Na_V1.9$-mediated current responses. In this context, DKO DRG neurons offer a huge technical advantage, enabling functional analysis of overexpressed human $Na_V1.8$ and $Na_V1.9$ channels in the absence of interfering endogenous TTXr channels. In particular, the heterologous expression and subsequent functional analysis of $Na_V1.9$ channels, which is notoriously difficult, benefits from using DKO DRG neurons for expression. As shown here, using mutant $Na_V1.9$-L811P channels associated with congenital analgesia and pruritus in humans,[37,62] such variants can be efficiently analyzed. Moreover, the absence of TTXr Na_V channels makes DKO DRG neurons a valuable tool to study nociceptor-specific TTXs Na^+ currents in their native environment without interfering TTXr current components.

Here, we describe a new TTXr-Na_V null mouse model with functional loss of 2 major Na_V subtypes preferentially expressed in peripheral sensory neurons. Our data imply that the $Na_V1.8$/

Table 1

Summary of behavior phenotype for $Na_V1.8$ KO, $Na_V1.9$ KO, and $Na_V1.8/Na_V1.9$ DKO mice.

	$Na_V1.8^{-/-}$	$Na_V1.9^{-/-}$	$Na_V1.8/Na_V1.9$ DKO
Phenotype (vs WT)	↓ noxious mechanical pressure sensitivity (Randall–Selitto)[3,46] ↑ cold preference[48] ↓ noxious cold sensitivity (cold plate 0°C, −5°C)[44,81] ↓ heat sensitivity (Hargreaves)[3]	↓ noxious mechanical pressure sensitivity (Randall–Selitto)[46] ↓ mechanical sensitivity (von Frey, *only on the left side*)[38] ↓ heat sensitivity (modified Hargreaves)[27] ↓ jumps to decreasing temperature plate[43] ↑ cold preference[43] ↑ latency to tail flick at 5°C[43]	↓ noxious mechanical pressure sensitivity (Randall–Selitto) (Fig. 7B)
Inflammatory pain	Carrageenan delayed onset,[3] normal[38] CFA normal[38] Formalin normal[38,51] NGF ↓ thermal hyperalgesia[31] PGE2 normal[31]	Carrageenan ↓ thermal and mechanical hyperalgesia,[42] normal[38] CFA ↓ thermal hyperalgesia[56]; normal[38] Formalin ↓ 2nd phase[38,42,56] MOA ↓ thermal and mechanical hyperalgesia[42] PGE2 ↓ thermal hyperalgesia[56]	Formalin normal (Figs. 8D and E)
Neuropathic pain	CCI ↓ cold hypersensitivity,[47] normal[38] PNL normal[31,51] SNI normal[38] SNT normal[47]	CCI ↓ cold hypersensitivity,[47] normal[38] Oxaliplatin ↓ cold hypersensitivity[43] SNI ↓ sensitivity to acetone[38] SNT normal.[47]	
Visceral pain	Nb nematode infection ↓excitability DRGs innervating the GI tract.[26]	Nb nematode infection normal.[26]	
In vitro Ex vivo	↓ responses to cooling and mechanical stimulation at low temperatures.[81]	↓ heat sensitivity in C-fibers and ↓ mechanosensitivity (skin nerve preparation)[27]; highly modulated by inflammatory mediators[6,45] Impaired response to cooling[43]	

CCI, chronic constriction injury; CFA, complete Freund adjuvant; MOA, complete Freund adjuvant–induced monoarthritis; NGF, nerve growth factor; PGE2, prostaglandin E2; PNL, peripheral nerve ligation; SNI spared nerve injury; SNT, spinal nerve transection.

$Na_V1.9$ DKO is well compensated despite significant alterations of sensory neuron anatomy and nociceptor excitability. Thus, $Na_V1.8/Na_V1.9$ DKO sensory neurons from spinal, enteric, or trigeminal ganglia are a valuable laboratory resource facilitating systematic functional studies of $Na_V1.8$ and $Na_V1.9$ channels and disease-associated variants.

Conflict of interest statement

The authors have no conflicts of interest to declare.

Acknowledgements

The authors wish to thank Kathrin Schorr, Sebastian Gießelmann, Ann-Katrin Hellberg-Schnieder, and Dr. Ana P. Luiz for technical assistance. This work was supported by the Genomics Facility and the Flow Cytometry Facility of the Interdisciplinary Centre for Clinical Research (IZKF) Aachen within the Faculty of Medicine at RWTH Aachen University.

This work was supported by grants from the Deutsche Forschungsgemeinschaft (DFG) to I.K. (KU1587/3-1, KU1587/4-1, and KU1587/10-1) and E.L. (LE2338/3-1 and LE2338/3-2). M.A.S., F.I., and Q.M. were supported by Versus Arthritis U.K. research grant (21950). The funders had no role in experimental design, data collection and analysis, decision to publish, or preparation of the manuscript.

Data availability statement: RNA Sequencing data will be deposited in NCBI's Gene Expression Omnibus and are accessible through GEO Series upon acceptance of the manuscript.

Parts of the data have been presented as a poster at the following meeting: The Challenge of Chronic Pain: from Genomics to Therapy, 29 November–1 December 2023, Wellcome Genome Campus, UK.

Supplemental digital content

Supplemental digital content associated with this article can be found online at http://links.lww.com/PAIN/C139.

Article history:
Received 20 November 2023
Received in revised form 26 July 2024
Accepted 30 July 2024
Available online 4 October 2024

References

[1] Abrahamsen B, Zhao J, Asante CO, Cendan CM, Marsh S, Martinez-Barbera JP, Nassar MA, Dickenson AH, Wood JN. The cell and molecular basis of mechanical, cold, and inflammatory pain. Science 2008;321:702–5.
[2] Akopian AN, Sivilotti L, Wood JN. A tetrodotoxin-resistant voltage-gated sodium channel expressed by sensory neurons. Nature 1996;379:257–62.
[3] Akopian AN, Souslova V, England S, Okuse K, Ogata N, Ure J, Smith A, Kerr BJ, McMahon SB, Boyce S, Hill R, Stanfa LC, Dickenson AH, Wood JN. The tetrodotoxin-resistant sodium channel SNS has a specialized function in pain pathways. Nat Neurosci 1999;2:541–8.
[4] Aleem AM, Jankun J, Dignam JD, Walther M, Kühn H, Svergun DI, Skrzypczak-Jankun E. Human platelet 12-lipoxygenase, new findings about its activity, membrane binding and low-resolution structure. J Mol Biol 2008;376:193–209.
[5] Amaya F, Decosterd I, Samad TA, Plumpton C, Tate S, Mannion RJ, Costigan M, Woolf CJ. Diversity of expression of the sensory neuron-specific TTX-resistant voltage-gated sodium ion channels SNS and SNS2. Mol Cell Neurosci 2000;15:331–42.
[6] Amaya F, Wang HB, Costigan M, Allchorne AJ, Hatcher JP, Egerton J, Stean T, Morisset V, Grose D, Gunthorpe MJ, Chessell IP, Tate S, Green PJ, Woolf CJ. The voltage-gated sodium channel Na(v)1.9 is an effector of peripheral inflammatory pain hypersensitivity. J Neurosci 2006;26:12852–60.
[7] Bateman A, Sandford R. The PLAT domain: a new piece in the PKD1 puzzle. Curr Biol CB 1999;9:R588–90.

[8] Bennett DL, Clark AJ, Huang J, Waxman SG, Dib-Hajj SD. The role of voltage-gated sodium channels in pain signaling. Physiol Rev 2019;99: 1079–151.
[9] Bhuiyan SA, Xu M, Yang L, Semizoglou E, Bhatia P, Pantaleo KI, Tochitsky I, Jain A, Erdogan B, Blair S, Cat V, Mwirigi JM, Sankaranarayanan I, Tavares-Ferreira D, Green U, McIlvried LA, Copits BA, Bertels Z, Del Rosario JS, Widman AJ, Slivicki RA, Yi J, Sharif-Naeini R, Woolf CJ, Lennerz JK, Whited JL, Price TJ, Robert W, Renthal W, Renthal W. Harmonized cross-species cell atlases of trigeminal and dorsal root ganglia. Sci Adv 2024;10:eadj9173. doi: 10.1126/sciadv.adj9173.
[10] Black JA, Frezel N, Dib-Hajj SD, Waxman SG. Expression of Nav1.7 in DRG neurons extends from peripheral terminals in the skin to central preterminal branches and terminals in the dorsal horn. Mol Pain 2012;8: 82.
[11] Blair NT, Bean BP. Roles of tetrodotoxin (TTX)-sensitive Na+ current, TTX-resistant Na+ current, and Ca2+ current in the action potentials of nociceptive sensory neurons. J Neurosci 2002;22:10277–90.
[12] Boudes M, Sar C, Menigoz A, Hilaire C, Péquignot MO, Kozlenkov A, Marmorstein A, Carroll P, Valmier J, Scamps F. *Best1* is a gene regulated by nerve injury and required for Ca^{2+}-activated Cl^- current expression in axotomized sensory neurons. J Neurosci 2009;29:10063–71.
[13] Cho H, Yang YD, Lee J, Lee B, Kim T, Jang Y, Back SK, Na HS, Harfe BD, Wang F, Raouf R, Wood JN, Oh U. The calcium-activated chloride channel anoctamin 1 acts as a heat sensor in nociceptive neurons. Nat Neurosci 2012;15:1015–21.
[14] Choi J-S, Waxman SG. Physiological interactions between $Na_v1.7$ and $Na_v1.8$ sodium channels: a computer simulation study. J Neurophysiol 2011;106:3173–84.
[15] Cong L, Ran FA, Cox D, Lin S, Barretto R, Habib N, Hsu PD, Wu X, Jiang W, Marraffini LA, Zhang F. Multiplex genome engineering using CRISPR/Cas systems. Science 2013;339:819–23.
[16] Cummins TR, Dib-Hajj SD, Black JA, Akopian AN, Wood JN, Waxman SG. A novel persistent tetrodotoxin-resistant sodium current in SNS-null and wild-type small primary sensory neurons. J Neurosci 1999; 19:RC43.
[17] Cummins TR, Howe JR, Waxman SG. Slow closed-state inactivation: a novel mechanism underlying ramp currents in cells expressing the hNE/PN1 sodium channel. J Neurosci 1998;18:9607–19.
[18] Deacon RMJ. Measuring motor coordination in mice. J Vis Exp 2013; 75: e2609. doi: 10.3791/2609
[19] Deng L, Dourado M, Reese RM, Huang K, Shields SD, Stark KL, Maksymetz J, Lin H, Kaminker JS, Jung M, Foreman O, Tao J, Ngu H, Joseph V, Roose-Girma M, Tam L, Lardell S, Orrhult LS, Karila P, Allard J, Hackos DH. Nav1.7 is essential for nociceptor action potentials in the mouse in a manner independent of endogenous opioids. Neuron 2023; 111:2642–59.e13.
[20] Elliott AA, Elliott JR. Characterization of TTX-sensitive and TTX-resistant sodium currents in small-cells from adult-rat dorsal-root ganglia. J Physiol 1993;463:39–56.
[21] Goodwin G, McMahon SB. The physiological function of different voltage-gated sodium channels in pain. Nat Rev Neurosci 2021;22:263–74.
[22] Grlickova-Duzevik E, Reimonn TM, Michael M, Tian T, Owyoung J, McGrath-Conwell A, Neufeld P, Mueth M, Molliver DC, Ward PJ, Harrison BJ. Members of the CUGBP Elav-like family of RNA-binding proteins are expressed in distinct populations of primary sensory neurons. J Comp Neurol 2023;531:1425–42.
[23] Ha GE, Lee J, Kwak H, Song K, Kwon J, Jung S-Y, Hong J, Chang G-E, Hwang EM, Shin H-S, Lee CJ, Cheong E. The Ca2+-activated chloride channel anoctamin-2 mediates spike-frequency adaptation and regulates sensory transmission in thalamocortical neurons. Nat Commun 2016;7:13791. doi: 10.1038/ncomms13791.
[24] Heinrich T, Hübner C, Kurth I. Isolation and primary cell culture of mouse dorsal root ganglion neurons. Bio Protocol 2016;6:e1785. doi: 10.21769/BioProtoc.1785
[25] Herzog RI, Cummins TR, Waxman SG. Persistent TTX-resistant Na+ current affects resting potential and response to depolarization in simulated spinal sensory neurons. J Neurophysiol 2001;86: 1351–64.
[26] Hillsley K, Lin J-H, Stanisz A, Grundy D, Aerssens J, Peeters PJ, Moechars D, Coulie B, Stead RH. Dissecting the role of sodium currents in visceral sensory neurons in a model of chronic hyperexcitability using $Na_v1.8$ and $Na_v1.9$ null mice: $Na_v1.8$ and $Na_v1.9$ in chronic hyperexcitability. J Physiol 2006;576:257–67.
[27] Hoffmann T, Kistner K, Carr RW, Nassar MA, Reeh PW, Weidner C. Reduced excitability and impaired nociception in peripheral unmyelinated fibers from Nav1.9-null mice. PAIN 2017;158:58–67.
[28] Hughes J, Smith TW, Kosterlitz HW, Fothergill LA, Morgan BA, Morris HR. Identification of two related pentapeptides from the brain with potent opiate agonist activity. Nature 1975;258:577–80.
[29] Jinek M, Chylinski K, Fonfara I, Hauer M, Doudna JA, Charpentier E. A programmable dual-RNA-guided DNA endonuclease in adaptive bacterial immunity. Science 2012;337:816–21.
[30] Jung M, Dourado M, Maksymetz J, Jacobson A, Laufer BI, Baca M, Foreman O, Hackos DH, Riol-Blanco L, Kaminker JS. Cross-species transcriptomic atlas of dorsal root ganglia reveals species-specific programs for sensory function. Nat Commun 2023;14:366.
[31] Kerr BJ, Souslova V, McMahon SB, Wood JN. A role for the TTX-resistant sodium channel Nav 1.8 in NGF-induced hyperalgesia, but not neuropathic pain. Neuroreport 2001;12:3077–80.
[33] Kupari J, Usoskin D, Parisien M, Lou D, Hu Y, Fatt M, Lönnerberg P, Spångberg M, Eriksson B, Barkas N, Kharchenko PV, Loré K, Khoury S, Diatchenko L, Ernfors P. Single cell transcriptomics of primate sensory neurons identifies cell types associated with chronic pain. Nat Commun 2021;12:1510.
[34] Lee B, Cho H, Jung J, Yang YD, Yang D-J, Oh U. Anoctamin 1 contributes to inflammatory and nerve-injury induced hypersensitivity. Mol Pain 2014;10:5.
[35] Leipold E, Borges A, Heinemann SH. Scorpion β-toxin interference with NaV channel voltage sensor gives rise to excitatory and depressant modes. J Gen Physiol 2012;139:305–19.
[36] Leipold E, Hanson-Kahn A, Frick M, Gong P, Bernstein JA, Voigt M, Katona I, Oliver Goral R, Altmüller J, Nürnberg P, Weis J, Hübner CA, Heinemann SH, Kurth I. Cold-aggravated pain in humans caused by a hyperactive NaV1.9 channel mutant. Nat Commun 2015;6:10049. doi: 10.1038/ncomms10049.
[37] Leipold E, Liebmann L, Korenke GC, Heinrich T, Gießelmann S, Baets J, Ebbinghaus M, Goral RO, Stödberg T, Hennings JC, Bergmann M, Altmüller J, Thiele H, Wetzel A, Nürnberg P, Timmerman V, De Jonghe P, Blum R, Schaible H-G, Weis J, Heinemann SH, Hübner CA, Kurth I. A de novo gain-of-function mutation in SCN11A causes loss of pain perception. Nat Genet 2013;45:1399–404.
[38] Leo S, D'Hooge R, Meert T. Exploring the role of nociceptor-specific sodium channels in pain transmission using Nav1.8 and Nav1.9 knockout mice. Behav Brain Res 2010;208:149–57.
[39] Li L, Rutlin M, Abraira VE, Cassidy C, Kus L, Gong S, Jankowski MP, Luo W, Heintz N, Koerber HR, Woodbury CJ, Ginty DD. The functional organization of cutaneous low-threshold mechanosensory neurons. Cell 2011;147:1615–27.
[40] Liu B, Linley JE, Du X, Zhang X, Ooi L, Zhang H, Gamper N. The acute nociceptive signals induced by bradykinin in rat sensory neurons are mediated by inhibition of M-type K+ channels and activation of Ca2+-activated Cl– channels. J Clin Invest 2010;120:1240–52.
[41] Löken LS, Wessberg J, Morrison I, McGlone F, Olausson H. Coding of pleasant touch by unmyelinated afferents in humans. Nat Neurosci 2009; 12:547–8.
[42] Lolignier S, Amsalem M, Maingret F, Padilla F, Gabriac M, Chapuy E, Eschalier A, Delmas P, Busserolles J. Nav1.9 channel contributes to mechanical and heat pain hypersensitivity induced by subacute and chronic inflammation. PLoS One 2011;6:e23083. doi: 10.1371/journal.pone.0023083.
[43] Lolignier S, Bonnet C, Gaudioso C, Noël J, Ruel J, Amsalem M, Ferrier J, Rodat-Despoix L, Bouvier V, Aissouni Y, Prival L, Chapuy E, Padilla F, Eschalier A, Delmas P, Busserolles J. The Nav1.9 channel is a key determinant of cold pain sensation and cold allodynia. Cell Rep 2015;11: 1067–78.
[44] Luiz AP, MacDonald DI, Santana-Varela S, Millet Q, Sikandar S, Wood JN, Emery EC. Cold sensing by $Na_v1.8$-positive and $Na_v1.8$-negative sensory neurons. Proc Natl Acad Sci 2019; 116:3811–16. doi: 10.1073/pnas.1814545116.
[45] Maingret F, Coste B, Padilla F, Clerc N, Crest M, Korogod SM, Delmas P. Inflammatory mediators increase Nav1.9 current and excitability in Nociceptors through a coincident detection mechanism. J Gen Physiol 2008;131:211–25.
[46] Minett MS, Eijkelkamp N, Wood JN. Significant determinants of mouse pain behaviour. PLoS One 2014;9:e104458. doi: 10.1371/journal.pone.0104458.
[47] Minett MS, Falk S, Santana-Varela S, Bogdanov YD, Nassar MA, Heegaard AM, Wood JN. Pain without nociceptors? Nav1.7-Independent pain mechanisms. Cell Rep 2014;6:301–12.
[48] Minett MS, Nassar MA, Clark AK, Passmore G, Dickenson AH, Wang F, Malcangio M, Wood JN. Distinct Nav1.7-dependent pain sensations require different sets of sensory and sympathetic neurons. Nat Commun 2012;3:791.

[49] Minett MS, Quick K, Wood JN. Behavioral measures of pain thresholds. Curr Protoc Mouse Biol 2011;1:383–412.
[50] Nagy A, editor. Manipulating the mouse embryo: a laboratory manual. 3rd ed. Cold Spring Harbor, NY: Cold Spring Harbor Laboratory Press, 2003.
[51] Nassar MA, Levato A, Stirling LC, Wood JN. Neuropathic pain develops normally in mice lacking both $Na_v1.7$ and $Na_v1.8$. Mol Pain 2005;1:24.
[52] Nassar MA, Stirling LC, Forlani G, Baker MD, Matthews EA, Dickenson AH, Wood JN. Nociceptor-specific gene deletion reveals a major role for Na(v)1.7 (PN1) in acute and inflammatory pain. Proc Natl Acad Sci USA 2004;101:12706–11.
[53] Naylor CE, Eaton JT, Howells A, Justin N, Moss DS, Titball RW, Basak AK. Structure of the key toxin in gas gangrene. Nat Struct Biol 1998;5: 738–46.
[54] Nguyen MQ, Von Buchholtz LJ, Reker AN, Ryba NJ, Davidson S. Single-nucleus transcriptomic analysis of human dorsal root ganglion neurons. eLife 2021;10:e71752. doi: 10.7554/eLife.71752.
[55] Olausson H, Lamarre Y, Backlund H, Morin C, Wallin BG, Starck G, Ekholm S, Strigo I, Worsley K, Vallbo ÅB, Bushnell MC. Unmyelinated tactile afferents signal touch and project to insular cortex. Nat Neurosci 2002;5:900–4.
[56] Priest BT, Murphy BA, Lindia JA, Diaz C, Abbadie C, Ritter AM, Liberator P, Iyer LM, Kash SF, Kohler MG, Kaczorowski GJ, MacIntyre DE, Martin WJ. Contribution of the tetrodotoxin-resistant voltage-gated sodium channel Na(v)1.9 to sensory transmission and nociceptive behavior. Proc Natl Acad Sci USA 2005;102:9382–7.
[57] Renganathan M, Cummins TR, Waxman SG. Contribution of Na(v)1.8 sodium channels to action potential electrogenesis in DRG neurons. J Neurophysiol 2001;86:629–40.
[58] Renganathan M, Dib-Hajj S, Waxman SG. Na(v)1.5 underlies the "third TTX-R sodium current" in rat small DRG neurons. Brain Res Mol Brain Res 2002;106:70–82.
[59] Rush AM, Bräu ME, Elliott AA, Elliott JR. Electrophysiological properties of sodium current subtypes in small cells from adult rat dorsal root ganglia. J Physiol 1998;511(Pt 3):771–89.
[60] Rush AM, Cummins TR, Waxman SG. Multiple sodium channels and their roles in electrogenesis within dorsal root ganglion neurons. J Physiol 2007;579:1–14.
[61] Sakai K, Sanders KM, Lin S-H, Pavlenko D, Funahashi H, Lozada T, Hao S, Chen C-C, Akiyama T. Low-threshold mechanosensitive VGLUT3-lineage sensory neurons mediate spinal inhibition of itch by touch. J Neurosci 2020;40:7688–701.
[62] Salvatierra J, Diaz-Bustamante M, Meixiong J, Tierney E, Dong X, Bosmans F. A disease mutation reveals a role for NaV1.9 in acute itch. J Clin Invest 2018;128:5434–47.
[63] Sangameswaran L, Delgado SG, Fish LM, Koch BD, Jakeman LB, Stewart GR, Sze P, Hunter JC, Eglen RM, Herman RC. Structure and function of a novel voltage-gated, tetrodotoxin-resistant sodium channel specific to sensory neurons. J Biol Chem 1996;271:5953–6.
[64] Santiago C, Sharma N, Africawala N, Siegrist J, Handler A, Tasnim A, Anjum R, Turecek J, Lehnert BP, Renauld S, Nolan-Tamariz M, Iskols M, Magee AR, Paradis S, Ginty DD. Activity-dependent development of the body's touch receptors. bioRxiv Preprint Server Biol 2023. doi: 10.1101/2023.09.23.559109
[65] Schröder JM, Hoheneck M, Weis J, Deist H. Ethylene oxide polyneuropathy: clinical follow-up study with morphometric and electron microscopic findings in a sural nerve biopsy. J Neurol 1985; 232:83–90.
[66] Seibenhener ML, Wooten MC. Use of the open field maze to measure locomotor and anxiety-like behavior in mice. J Vis Exp 2015; 96: 52434.doi: 10.3791/52434.
[67] Sharma N, Flaherty K, Lezgiyeva K, Wagner DE, Klein AM, Ginty DD. The emergence of transcriptional identity in somatosensory neurons. Nature 2020;577:392–8.
[68] Simantov R, Snyder SH. Morphine-like peptides in mammalian brain: isolation, structure elucidation, and interactions with the opiate receptor. Proc Natl Acad Sci USA 1976;73:2515–9.
[69] Stephan AB, Shum EY, Hirsh S, Cygnar KD, Reisert J, Zhao H. ANO2 is the cilial calcium-activated chloride channel that may mediate olfactory amplification. Proc Natl Acad Sci USA 2009;106:11776–81.
[70] Tate S, Benn S, Hick C, Trezise D, John V, Mannion RJ, Costigan M, Plumpton C, Grose D, Gladwell Z, Kendall G, Dale K, Bountra C, Woolf CJ. Two sodium channels contribute to the TTX-R sodium current in primary sensory neurons. Nat Neurosci 1998;1:653–5.
[71] Tavares-Ferreira D, Shiers S, Ray PR, Wangzhou A, Jeevakumar V, Sankaranarayanan I, Cervantes AM, Reese JC, Chamessian A, Copits BA, Dougherty PM, Gereau RW, Burton MD, Dussor G, Price TJ. Spatial transcriptomics of dorsal root ganglia identifies molecular signatures of human nociceptors. Sci Transl Med 2022;14:eabj8186. doi: 10.1126/scitranslmed.abj8186.
[72] Trouillet A, Miller KK, George SS, Wang P, Ali N-E-S, Ricci A, Grillet N. Loxhd1 mutations cause mechanotransduction defects in cochlear hair cells. J Neurosci 2021;41:3331–43.
[73] Truett GE, Heeger P, Mynatt RL, Truett AA, Walker JA, Warman ML. Preparation of PCR-quality mouse genomic DNA with hot sodium hydroxide and Tris (HotSHOT). BioTechniques 2000;29:52–4.
[74] Usoskin D, Furlan A, Islam S, Abdo H, Lonnerberg P, Lou D, Hjerling-Leffler J, Haeggstrom J, Kharchenko O, Kharchenko PV, Linnarsson S, Ernfors P. Unbiased classification of sensory neuron types by large-scale single-cell RNA sequencing. Nat Neurosci 2015;18:145–53.
[75] Vanoye CG, Kunic JD, Ehring GR, George AL. Mechanism of sodium channel NaV1.9 potentiation by G-protein signaling. J Gen Physiol 2013; 141:193–202.
[76] Wang H, Cao Z, Jiang X, Huang C, Cao C, Liu Z. Tlx3 controls the development of C-low threshold mechanoreceptors. NeuroReport 2022; 33:617–22.
[77] Yang YD, Cho H, Koo JY, Tak MH, Cho Y, Shim W-S, Park SP, Lee J, Lee B, Kim B-M, Raouf R, Shin YK, Oh U. TMEM16A confers receptor-activated calcium-dependent chloride conductance. Nature 2008;455: 1210–5.
[78] Yoo S, Santos C, Reynders A, Marics I, Malapert P, Gaillard S, Charron A, Ugolini S, Rossignol R, El Khallouqi A, Springael J-Y, Parmentier M, Saurin AJ, Goaillard J-M, Castets F, Clerc N, Moqrich A. TAFA4 relieves injury-induced mechanical hypersensitivity through LDL receptors and modulation of spinal A-type K+ current. Cell Rep 2021;37:109884. doi: 10.1016/j.celrep.2021.109884.
[79] Zeisel A, Hochgerner H, Lönnerberg P, Johnsson A, Memic F, Van Der Zwan J, Häring M, Braun E, Borm LE, La Manno G, Codeluppi S, Furlan A, Lee K, Skene N, Harris KD, Hjerling-Leffler J, Arenas E, Ernfors P, Marklund U, Linnarsson S. Molecular architecture of the mouse nervous system. Cell 2018;174:999–1014.e22.
[80] Zhou X, Xiao Z, Xu Y, Zhang Y, Tang D, Wu X, Tang C, Chen M, Shi X, Chen P, Liang S, Liu Z. Electrophysiological and pharmacological analyses of Nav1.9 voltage-gated sodium channel by establishing a heterologous expression system. Front Pharmacol 2017;8:852.
[81] Zimmermann K, Leffler A, Babes A, Cendan CM, Carr RW, Kobayashi J, Nau C, Wood JN, Reeh PW. Sensory neuron sodium channel Nav1.8 is essential for pain at low temperatures. Nature 2007;447:855–8.